Instituto de Astronomia, Geofísica e Ciências Atmosféricas da Universidade de São Paulo (IAG-USP)

Joint inversion of receiver function and dispersion curves of surface waves in Uruguay

Martín Rodríguez Kacevas

2024

Martín Rodríguez Kacevas

Joint inversion of receiver function and dispersion curves of surface waves in Uruguay

Dissertation presented to the Department of Geophysics of the Institute of Astronomy, Geophysics and Atmospheric Sciences of the University of São Paulo as a partial requirement for obtaining the title of Master of Science.

Advisor: Prof. PhD. Marcelo Sousa de Assumpção

São Paulo

2024

Acknowledgements

First of all, I would like to thank my family for all the support provided during these two years of my master's degree.

I would also like to thank my advisor Prof. PhD. Marcelo Sousa de Assumpção for the support, trust, guidance, fruitful discussions and contribution of his great knowledge during these two years, without which it would not have been possible to carry out this master's dissertation.

I would like to thank PhD. Leda Sánchez Bettucci for her support, trust and knowledge during all these years without which my development in seismology would not have been possible.

I also thank all my colleagues at the IAG for the support, advice and good times during these years.

Finally, I would like to thank CAPES (Coordenação de Aperfeiçoamento de Pessoal de Nível Superior) for the master's scholarship that allowed my stay in São Paulo and therefore the development of this work.

Abstract

The development of a seismic network in Uruguay in recent years has enabled studies of crustal structure in a region with few seismological studies of this type. In this work, we update the crustal thicknesses and Vp/Vs ratios calculated by H-k stack and present S-wave velocity models based on joint inversion of receiver functions and Rayleigh wave group velocity dispersion curves.

Some interesting results are the presence of a lower crust with a high S-wave velocity of 4.1 km/s below one of the stations located on the Río de la Plata Craton and the existence of a transitional Moho in Uruguay's northernmost station on the Paraná Basin, perhaps suggesting the presence of localized underplated material. A relatively thick crust, 41.8 km, compared to surrounding stations, was found beneath the Sierra Ballena Shear Zone in the Dom Feliciano Belt. We confirm the decrease in crustal thickness when approaching the oceanic coast, reaching a Moho depth of 36.3 km in SE Uruguay. Finally, the calculated Poisson's ratio allows inferring a crust of felsic to intermediate composition beneath most of Uruguay.

Table of Contents

List of Tables

List of Figures

1. Introduction

The study of the structure of the crust and lithosphere is important to understand the tectonic evolution of any continental region. In Uruguay, seismological studies with this objective were only recently carried out. Most of them used the receiver function method (Rodríguez et al., 2017; 2019; Rivadeneyra-Vera et al., 2019; Rodríguez Kacevas, 2021; Rodríguez et al., 2022), but also Castro Valle (2021) made use of ellipticity curves calculated from seismic noise and earthquakes to generate velocity models from three broadband stations.

The aforementioned studies were made feasible by the recent installation of numerous broadband stations. These installations are a result of local initiatives spearheaded by the Geophysical Observatory of Uruguay (OGU), which presented a research project to CSIC (Comisión Sectorial de Investigación Científica, Universidad de la República), and various regional partnerships such as the "3 Basins" project, focusing on the Pantanal-Chaco-Paraná Basins (PCPB), in collaboration with the University of São Paulo. Additionally, international collaborations like the project with CAGS (Chinese Academy of Geological Sciences) have contributed to ongoing research, as the "Three Basins" project, and other national projects.

1.1. Purpose of this study

Since seismology studies are recent in Uruguay, there are no local seismic wave velocity models for the entire country. Therefore, obtaining S-wave velocity models for the Uruguayan crust and upper mantle was the main motivation of this study. Having reliable seismic wave velocity models allows a wide range of seismological studies to be carried out in Uruguay that until now was not possible. An additional objective was to obtain better estimates of the Vp/Vs ratio of the crust and Moho depth, that would also help to evaluate the reliability of the S-wave velocity models.

1.2. Stations

Eight broadband stations have been installed in Uruguayan territory as a result of the various projects mentioned. Table 1 provides a summary of the primary data from the stations utilized in this study, encompassing sensor and digitizer types, recording duration, and the percentage of available data. Figure 1 shows the distribution of

broadband stations and the main tectonic units in Uruguay. In addition, a more detailed analysis of the records of each station using obspy-scan plotting routine, showing gaps and overlaps, is provided in the appendix 6.1. Stations OGAUY and ROST had two different periods of operation. In addition, during its first period of operation, ROST station worked correctly only in the first six months of operation, after that period a malfunction in the sensor was noted. Also, Probabilistic Power Spectral Densities (PPSD) or noise curves were performed for each station using approximately three months of data (see appendix 6.1).

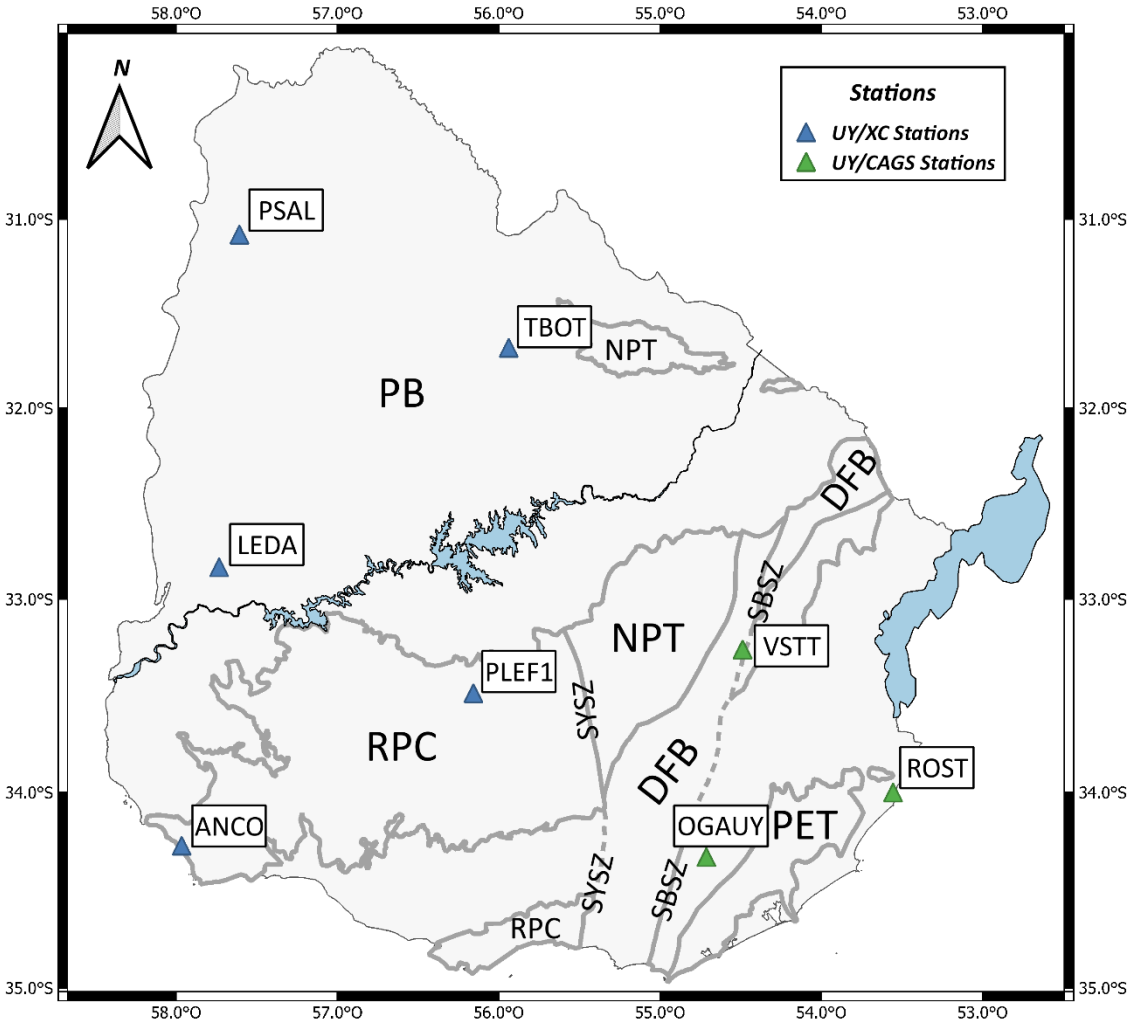

Figure 1: *Simplified tectonic sketch of Uruguay (modified from Sánchez Bettucci et al., 2010; Hueck et al., 2018) showing the main tectonic units and also the broadband stations used in this study. PB: Paraná Basin; RPC: Río de la Plata*

Craton; DFB: Dom Feliciano Belt; NPT: Nico Pérez Terrane; PET: Punta del Este Terrane; SYSZ: Sarandí del Yí Shear Zone; SBSZ: Sierra Ballena Shear Zone.

Table 1: Summary of the main data from the stations to be used in this research.

Station	Latitude	Longitude	Elevation (m)	Sensor	Digitizer	Recording time	% available data
OGAUY	-34.333	-54.712	252	Guralp 40T Guralp 3T	Guralp CD24-S3EAM Reftek 130	23/05/16 – 08/11/16 10/04/22 – 09/04/23	83.9 % 100 %
TBOT	-31.682	-55.937	171	Nanometrics Trillium 120QA	Centaur 3	11/01/17 – 01/09/19	87.4 %
ROST	-34.001	-53.554	30	Guralp 3T Nanometrics Trillium 120QA	Reftek 130 Centaur 3	10/10/21 – 08/04/23 21/07/23 – Present	99.6 % 76.3 %
VSTT	-33.262	-54.487	49	Guralp 3T	Reftek 130	16/10/21 – 06/04/23	96.5 %
ANCO	-34.275	-57.965	15	Nanometrics Trillium Compact 120s	Centaur 3	08/11/18 – Present	76.7 %
PSAL	-31.082	-57.607	62	Nanometrics Trillium 120QA	Centaur 3	31/01/18 – Present	78.8 %
PLEF1	-33.489	-56.156	103	Nanometrics Trillium Compact Horizon 120s	Centaur 3	18/03/22 – Present	96.7 %
LEDA	-32.834	-57.733	54	Nanometrics Trillium Compact Horizon 120s	Centaur 3	19/11/22 – Present	100 %

2. Geological Setting

The geological diversity of Uruguay, despite its small territory, makes it interesting to carry out a local study of this type. Three main tectonic units are found in Uruguay, these are the Paraná Basin (PB) in the north of the country, the Río de la Plata Craton (RPC) in the southwest and the Dom Feliciano Belt (DFB) located in the southeast. In addition, other smaller units are found within the limits of these units or around them, such as the Nico Pérez Terrane (NPT) and the Punta del Este Terrane (PET). All of these units present different characteristics both from a geological and geochronological point of view, with ages ranging from the Cenozoic in the Paraná Basin to the Archean in the Nico Pérez Terrain. A simplified tectonic sketch of Uruguay is presented in figure 1, showing the distribution of the aforementioned units, as well as the broadband stations used in this study.

2.1. Río de la Plata Craton

The Rio de la Plata Craton was originally defined by Almeida et al., (1973) to encompass the outcropping rocks of Precambrian age of the Montevideo formation, the Río de la Plata Region and Buenos Aires Province. The outcropping part of the Río de la Plata Craton is present mainly in the southwest and center of Uruguay (Oyhantçabal et al., 2011; 2018) and in small portions in southeastern Argentina in the Tandilia System (Cingolani, 2011). The total extension of the Craton is not defined since most of it is covered by Phanerozoic sediments, and therefore its northern limit is not known. However, evidence of its presence has been found to the west in drillings in the surroundings of the Sierras Pampeanas near Cordoba (Oyhantçabal et al., 2011). Figure 2 shows the proposed extension of the Craton across Argentina and Uruguay by Oyhantçabal et al., (2018).

The outcrop sector of the RPC in Uruguay corresponds to the Piedra Alta Terrane (Figure 2), of Paleoproterozoic age, which is composed mainly of a granitic-gneissic belt and two supracrustal metamorphic belts to the north and south of the granite-gneiss belt. Finally, the Florida Dolerite Dike Swarm (also known as Uruguayan dike swarm), of late Paleoproterozoic age ≈1790 Ma intrudes the granitic-gneissic belt.

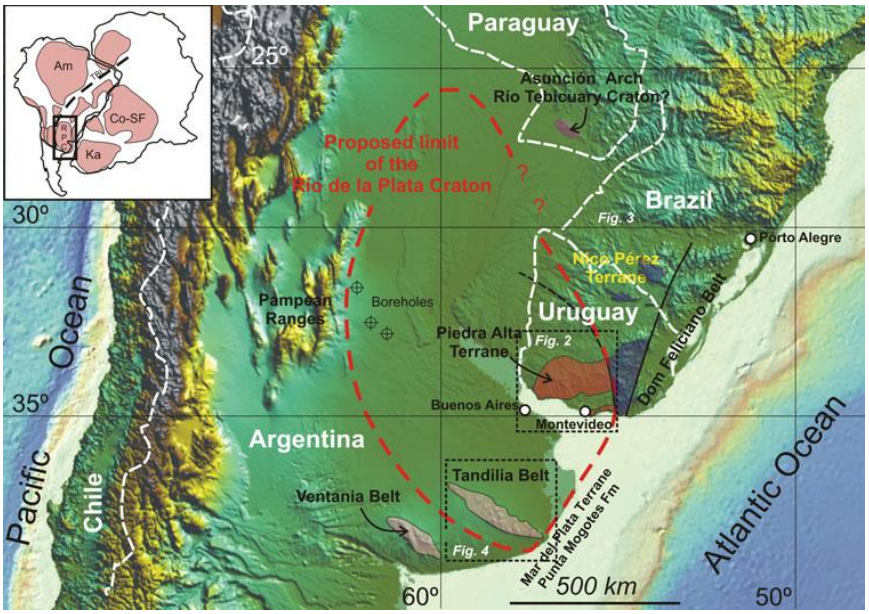

Figure 2: Extension of the Río de la Plata Craton in Argentina and Uruguay showing the main outcrop locations (Taken from Oyhantçabal et al., 2018).

2.2. Dom Feliciano Belt

Fragoso Cesar (1980) originally defined the Dom Feliciano Belt as a SW-NE oriented mobile belt found in eastern Uruguay and southern Brazil (Figure 3). This belt is the result of the transition from a convergent regime to a subsequent transcurrent. It was formed in the Neoproterozoic during the Brasiliano orogenic cycle due to the interaction of several cratons (Rio de la Plata, Congo, Kalahari) and several smaller terranes placed along main shear zones (Hueck et al., 2018).

Oriolo et al., (2016) divides this belt into two domains separated by the Sierra Ballena Shear Zone, in its Uruguayan portion. The western domain comprises mostly metavolcano-sedimentary units, basement inliers of the Nico Perez Terrane and granitoids while the eastern domain is composed in large proportion by granitoids of the Aigua Batolith and the Punta del Este Terrane, whose basement is composed of high-grade metamorphic rocks, with protoliths that yield ages c 800 Ma – 770 Ma (Hueck et al., 2018). In addition, the aforementioned Nico Perez Terrane acted as the cratonic foreland during the formation of this belt. This terrane is limited to the west by the Sarandí del Yí Shear Zone, which separates it from the Piedra Alta Terrane (Rio de la Plata Craton), while to the north is the boundary with the Paraná Basin. NPT rocks

present a wide range of ages from Archean to Paleoproterozoic and also underwent extensive reworking during the Neoproterozoic.

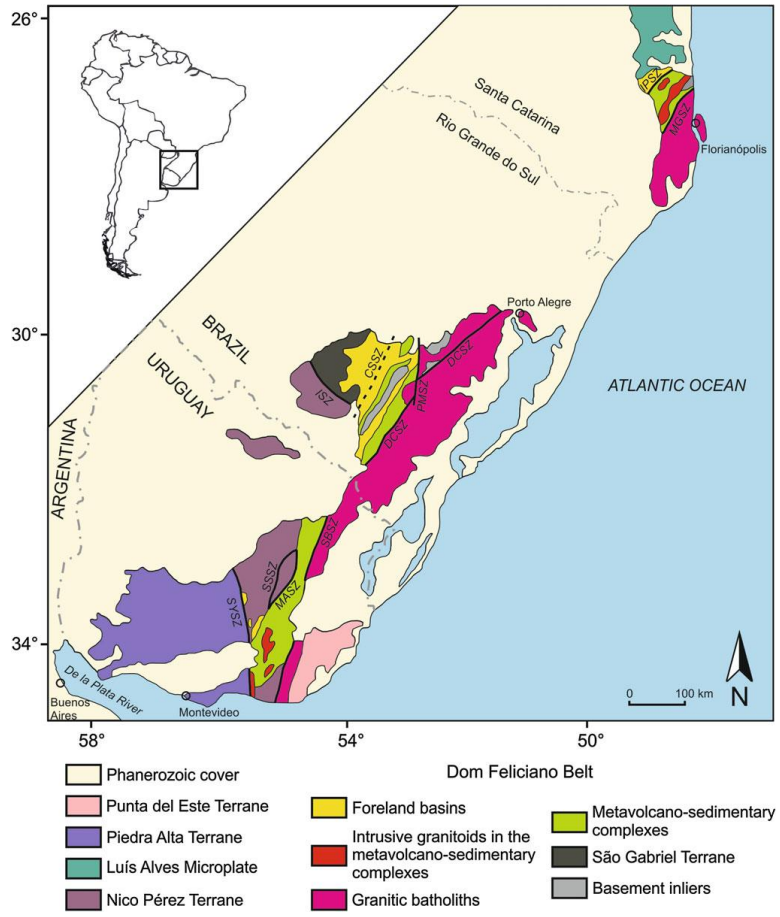

Figure 3: Tectonic map of the Dom Feliciano Belt (Taken from Hueck et al., 2018).

2.3. Paraná Basin

The Paraná Basin is an elliptical intracratonic basin whose approximate trend is SW – NE, which is located in the southeast of the South American continent and covers an area close to 1,400,000 km^2 that includes portions of the territories of Brazil, Paraguay, Argentina and Uruguay (Figure 4). The origin of this basin occurs in the late Ordovician in the interior of Gondwana and reaches thicknesses of up to 7000 meters in its central portion in Brazil (Milani & Thomaz Filho, 2000). Perhaps one of the most outstanding features of this basin is the presence of one of the largest episodes of basaltic magmatism recorded during the Mesozoic whose name is the Magmatic Province of Paraná, or Paraná – Etendeka for its counterpart in Africa with volumes of about 1,000,000 m^3 (Peate, 1997; Muzio, 2004).

In Uruguay, this basin covers an area of approximately 90.000 km^2. The depth of the basin in Uruguay increases towards the NW. The basement in the vicinity of Tacuarembó is between 300 and 700 meters deep, while to the west in the vicinity of the Uruguay River it is at a depth close to 1000 meters. In the NW sector of Uruguay, the thickness of the basin increases to approximately 3000 meters, as can be noted in the well information presented in Santa Ana et al. (2006) (see appendix 6.2). The geology of this basin in Uruguay varies depending on the sector, but in a simplified way it can be said that there are Paleozoic sediments at the base and towards the top there are, depending on the sector, basalts of the Arapey Formation of Mesozoic age and sandstones of the Tacuarembó Formation that often appear interspersed. These last two units are correlated with the Serra Geral and Botucatu Formations of Brazil, respectively.

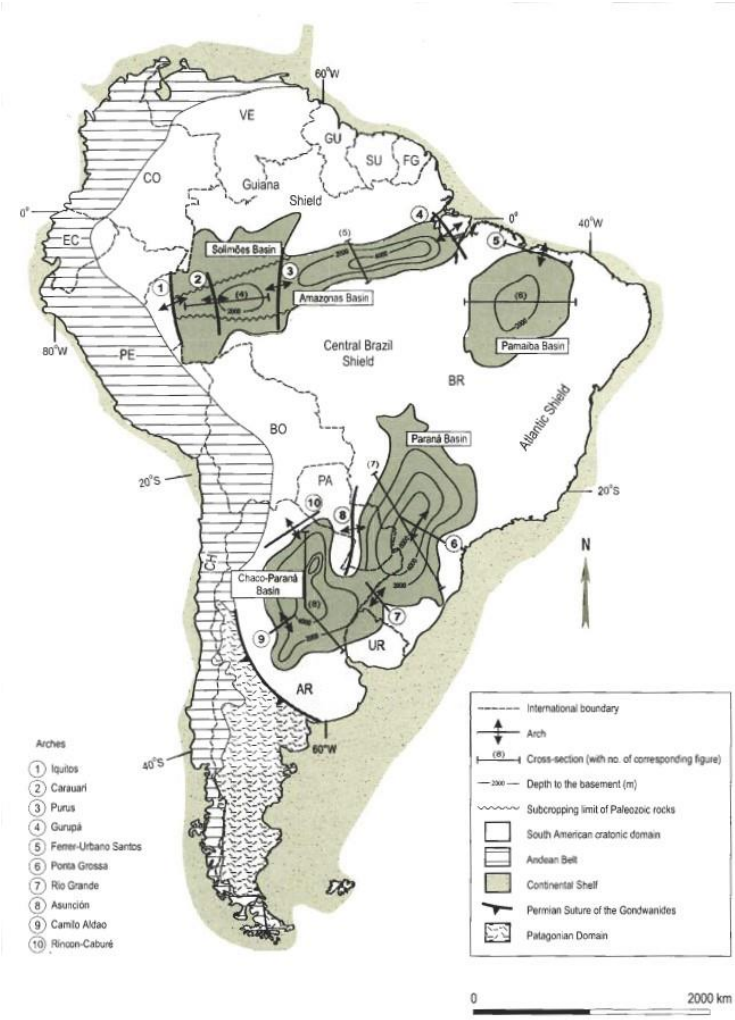

Figure 4: Location of the Paraná Basin in southeast South America (Taken from Milani & Thomas Filho, 2000).

3. Methodology, data selection and processing

3.1. Receiver Function

3.1.1. Overview

The receiver function method is a commonly utilized technique for gaining insights of the structure of the Earth's crust beneath a broadband station. When a steeply incident teleseismic P-wave encounters an interface between two media with significant property differences beneath a station, such as the Moho boundary, it generates a Ps phase. This Ps phase, converted from the direct P-wave, arrives at the receiver a few seconds after the direct P-wave on the seismogram. By analyzing the time lag between the P-wave and the Ps-wave, the depth of the discontinuity that produced the Ps phase can be estimated. However, detecting the Ps wave in seismograms proves challenging as it tends to be obscured within the coda of the direct P-wave.

Using an almost vertically incident teleseismic P waves at the interface implies that virtually all of the P-wave energy will be recorded in the vertical component of the seismogram, while P to S conversions predominate in the radial component (Langston, 1977). A receiver function is essentially a time series that records the seismic wave arrivals from various phases that have interacted with subsurface structures within the Earth's crust and upper mantle. The convolution of this time series with the vertical component of a seismogram reproduces the horizontal components of the seismogram (Langston, 1977; Ligorría & Ammon, 1999). Langston (1979) proposed a method for isolating the response of the Earth's structure beneath the station from source and instrument effects:

$$D_V(t) = I(t) * S(t) * E_V(t)$$

$$D_R(t) = I(t) * S(t) * E_R(t)$$

$$D_T(t) = I(t) * S(t) * E_T(t)$$

where S(t) is the effective source time function of the of the incident wave, I(t) is the instrumental response and $E_V(t)$, $E_R(t)$ and $E_T(t)$ are the vertical, radial and tangential receiver functions, respectively. Then it was assumed that $E_V(t) \approx \delta(t)$. With $\delta(t)$ being the Dirac delta function. So, we have:

$$I(t) * S(t) \simeq D_V(t)$$

So, in the frequency domain we can find $E_R(w)$ and $E_T(w)$ through the following deconvolution (spectral division):

$$E_R(w) = \frac{D_R(w)}{I(w)S(w)} \simeq \frac{D_R(w)}{D_V(w)}$$

$$E_T(w) = \frac{D_T(w)}{I(w)S(w)} \simeq \frac{D_T(w)}{D_V(w)}$$

and then transform $E_R(w)$ and $E_T(w)$ back into the time domain.

Figure 5 show the model of layer over a half-space with the conversion from P to S, the multiples (or reverberations) and a theoretical receiver function with the direct P-wave, Ps phase and the reverberations.

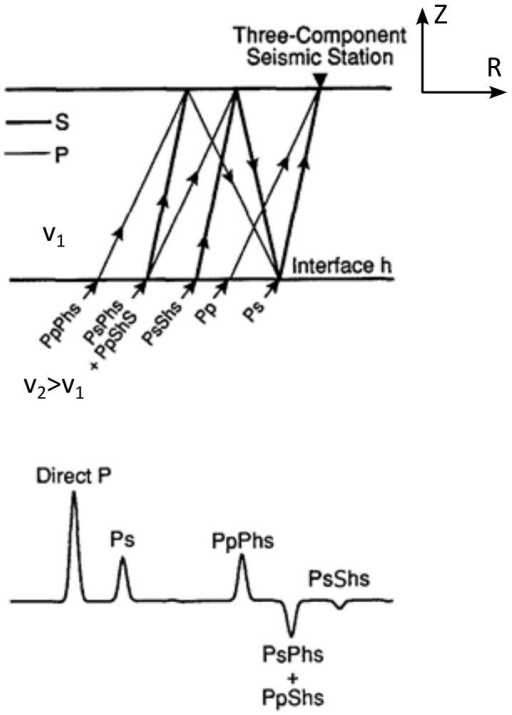

Figure 5: Diagram of a receiver function for a model of layer over a half-space. The surface layer has velocity v_1 and the half-space has velocity v_2. The main phases converted in the h interface are shown (Modified from Ammon, 1991).

3.1.2. Event selection, preprocessing and processing

Figures 6, 7, and 8 present the flowcharts related to event selection, preprocessing, and processing for the receiver function method.

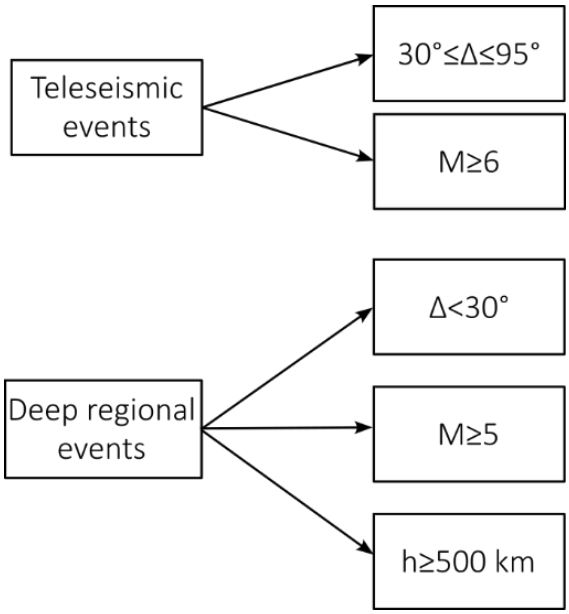

Figure 6: Seismic event selection criteria to perform receiver functions. Magnitudes greater than 5 or 6 were selected to ensure good signal to noise ratio.

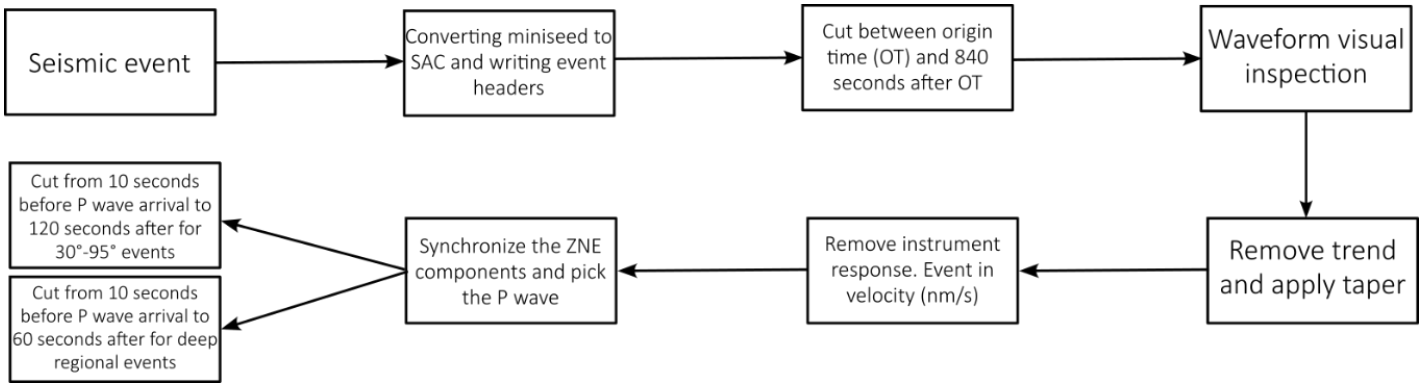

Figure 7: Earthquake preprocessing stage to apply receiver function method. All steps described in the flowchart were carried out using the SAC software: Seismic Analysis Code (Goldstein & Snoke, 2005; Goldstein et al., 2003).

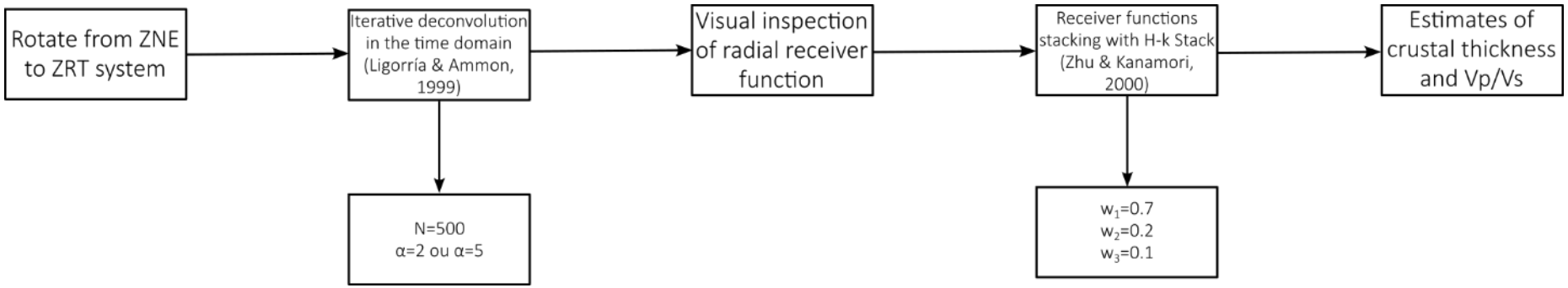

Figure 8: Processing phase of the previously pre-processed seismic event. Iterative deconvolution was performed with the saciterd program included in Computer Programs in Seismology (Herrmann, 2013). P-wave radial receiver functions that have reached the visual inspection phase are those that reproduced more than 85% of the signal after iterative deconvolution.

3.2. H-k Stacking

Zhu and Kanamori (2000) developed a receiver function stacking algorithm to calculate crustal thickness (H) and Vp/Vs (k) ratio. It consists in summing the amplitudes of the receiver functions at the theoretical arrival times of Ps, PpPs and PpSs+PsPs (the latter two phases are usually called multiples or reverberations) for different crustal thicknesses (H) and Vp/Vs, considering that the algorithm transforms the time domain waveforms into H-k domain.

Additionally, they pointed out that the use of multiples reduces the trade-off between crustal thickness and seismic wave velocities in the crust. While previous works estimated crustal thickness solely from the delay time of the Ps phase converted in the Moho.

Zhu and Kanamori (2000) highlighted several benefits of the algorithm. Firstly, it allows for the stacking of a significant number of events. Secondly, it is not necessary to select the arrival times of converted phases. Lastly, it yields an average crustal model by incorporating events with varying ray parameters (distance) and backazimuths.

A grid search is performed to find the H-k values that produce the largest stacked amplitude of Ps and reverberations, using the following equation:

$$S(H,k) = \sum_{i=1}^{n} w_1 r_i(t_1) + w_2 r_i(t_2) + w_3 r_i(t_3)$$

- w_1, w_2 and w_3 are weights that correspond to the contributions of the Ps, PpPs and PpSs+PsPs phases, respectively.
- $w_1 + w_2 + w_3 = 1$; generally, $w_1 \geq 0.7$ since it is the weight that corresponds to the Ps phase.
- $r_i(t_1)$, $r_i(t_2)$ and $r_i(t_3)$ are the amplitude values corresponding to the i-th trace of the radial receiver function for the predicted arrival times (t_1, t_2 and t_3) of phases Ps, PpPs and PpSs+PsPs, respectively.

To calculate t_1, t_2 and t_3 the following equations are used:

$$t_1 = H\left[\sqrt{\frac{k^2}{V_P^2} - p^2} - \sqrt{\frac{1}{V_P^2} - p^2}\right]$$

$$t_2 = H\left[\sqrt{\frac{k^2}{V_P^2} - p^2} + \sqrt{\frac{1}{V_P^2} - p^2}\right]$$

$$t_3 = 2H\left[\sqrt{\frac{k^2}{V_P^2} - p^2}\right]$$

where Vp is the average velocity of P waves in the crust and p is the ray parameter.

The function S(H,k) reaches a maximum when the 3 phases are stacked coherently with the correct values of H and k (Zhu & Kanamori, 2000). The H-k Stack program (Julià, 2003) was used to calculate crustal thickness and Vp/Vs ratio.

3.3. Dispersion Curves

3.3.1. Phase and group velocities

Most broadband seismograms are dominated by waves of large amplitude and low frequencies that arrive after the direct P and S waves. These are the surface waves that have the property of being dispersive, which means that at different periods/frequencies propagate at different velocities. This property is useful to know the variations in the physical properties of the crust and lithosphere. In general terms, low frequencies (longer periods) present higher velocities and vice versa. Another important characteristic of these waves is that low frequencies sample deeper parts of the earth, while high frequencies better sample shallow areas. The arrival time of dispersive waves at a receiver depends on the phase velocity (c) in each period (or frequency). While the group velocity (U) refers to the velocity at which the entire group of waves is traveling.

The phase velocity of a wave is the velocity at which a peak or trough moves and can be described by the following equation:

$$c = w/k$$

The group velocity of a wave is the velocity at which the overall shape of the wave's amplitudes, known as the wave's envelope, propagates through the medium. It can be described through the following equation:

$$U = \partial w/\partial k$$

The relationship between phase velocity and group velocity can be described by the following equations:

$$U = c - \lambda \left(\frac{dc}{dw}\right)$$

$$U = c \left(1 - k\frac{dc}{dw}\right)^{-1}$$

In the equations above: w is the angular frequency of the wave, k is the wave number and λ is the wavelength.

3.3.2. Multiple filter technique

Dispersion curves are graphical representations that show the variation of group velocity or phase velocity as a function of period or frequency. This group of curves represents various wave modes, from the fundamental mode to the higher modes and are representative of the average velocity between the event and the station.

The multiple filtering technique or MFT (Dziewonski et al., 1969; Herrin & Goforth, 1977) is a method that allows to obtain group velocity dispersion curves of Rayleigh or Love waves from a seismic event. The MFT is used to study variations of amplitude or energy of a signal as a function of velocity and period (Dziewonski et al., 1969).

It consists of applying a series of narrow Gaussian filters centered on different central frequencies that allow in a certain way "slicing" the surface waves of the seismic event. When applying each filter, the waveform transforms in a series of isolated wave packets and each of them has its envelope calculated (Figure 9). The envelope with the greatest amplitude usually corresponds to the fundamental mode, and other envelopes, of smaller amplitude, are also calculated that could correspond to different modes or simply noise present in the waveform. Generally, it is possible to recognize the fundamental mode, but it is more difficult to identify other modes. Then, the group velocity, for each period (or frequency), is determined by dividing the epicentral distance by the travel time of the wave packet.

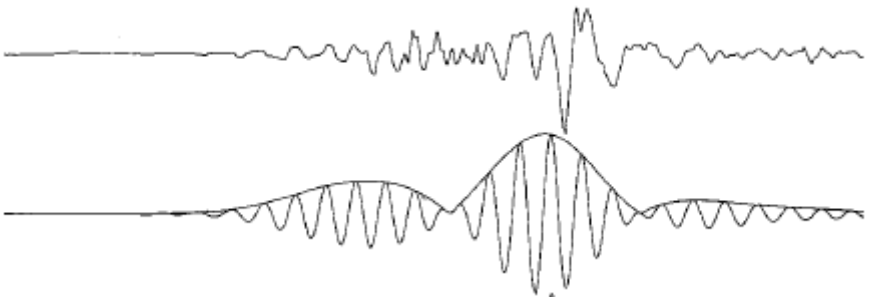

Figure 9: Unfiltered seismogram (top). Seismogram filtered in the frequency domain for a period of 10 seconds (bottom). The maximum amplitude of the envelopes corresponds to the first mode and the fundamental mode. (Taken from Dziewonski et al., 1969).

The do_mft program from Computer Programs in Seismology package (Herrmann, 2013) was used to apply this technique. The Gaussian filter used is the following:

$$H(w) = e^{-\alpha\frac{(w-w_0)^2}{(w_0)^2}}$$

Being α the width of the Gaussian filter and ω_0 the central frequency. Herrmann and Ammon (2002) recommends that the value of α changes with the epicentral distance:

Table 2: Relationship between α and epicentral distance

Distance Range	α
1000	25
2000	50
4000	100
8000	200

3.3.3. Regionalization

After generating the group velocity dispersion curves, they must be regionalized to be used in the joint inversion. Regionalized dispersion curves for each station were obtained from a tomography model of SE South America by Moura et al. (2024), which use the FMST (Fast Marching Surface Tomography) package (Rawlinson, 2005). The degrees calculated with a resolution of 1° x 1° and formats calculated for periods between 9 – 200 seconds, for all of South America. The regularization parameters for the inversion, η, which determines the smoothing, and ε, that determines the damping, were calculated with the test of the L curve (e.g. Aster et al., 2018), which fixes one parameter while varying the other.

3.3.4. Event selection, preprocessing and processing

Figures 10, 11, and 12 present the flowcharts related to event selection, preprocessing, and processing to generate group velocity dispersion curves using multiple filter technique.

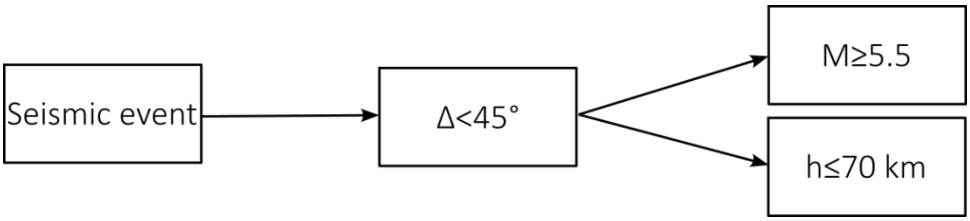

Figure 10: Seismic event selection criteria to perform group velocity dispersion curves. A magnitude of 5.5 or higher was chosen to ensure a good signal-to-noise ratio. In addition, events with hypocenters at depths less than 70 km were chosen to ensure "well-developed" surface wave trains.

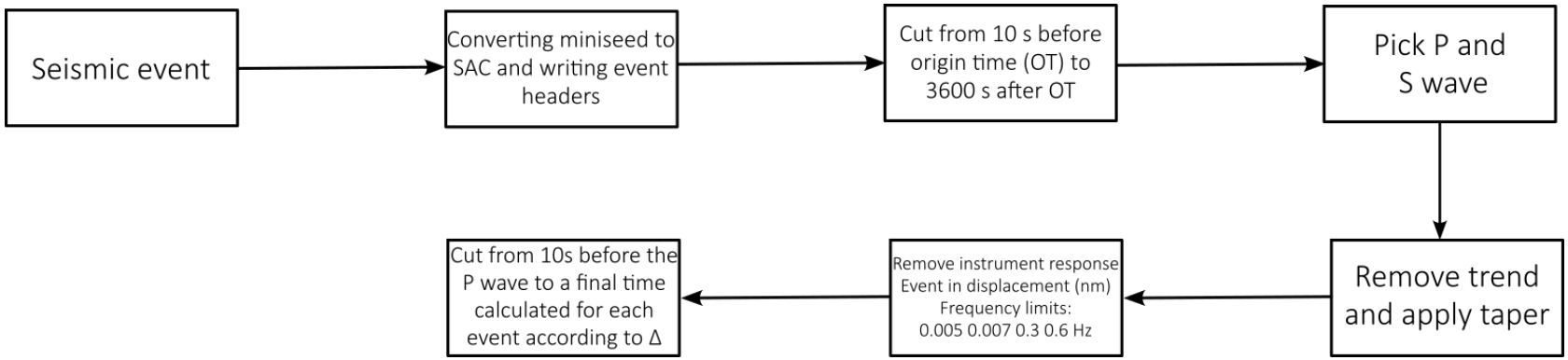

Figure 11: Earthquake preprocessing stage to apply multiple filtering technique (MFT). All steps described in the flowchart were carried out using the SAC software.

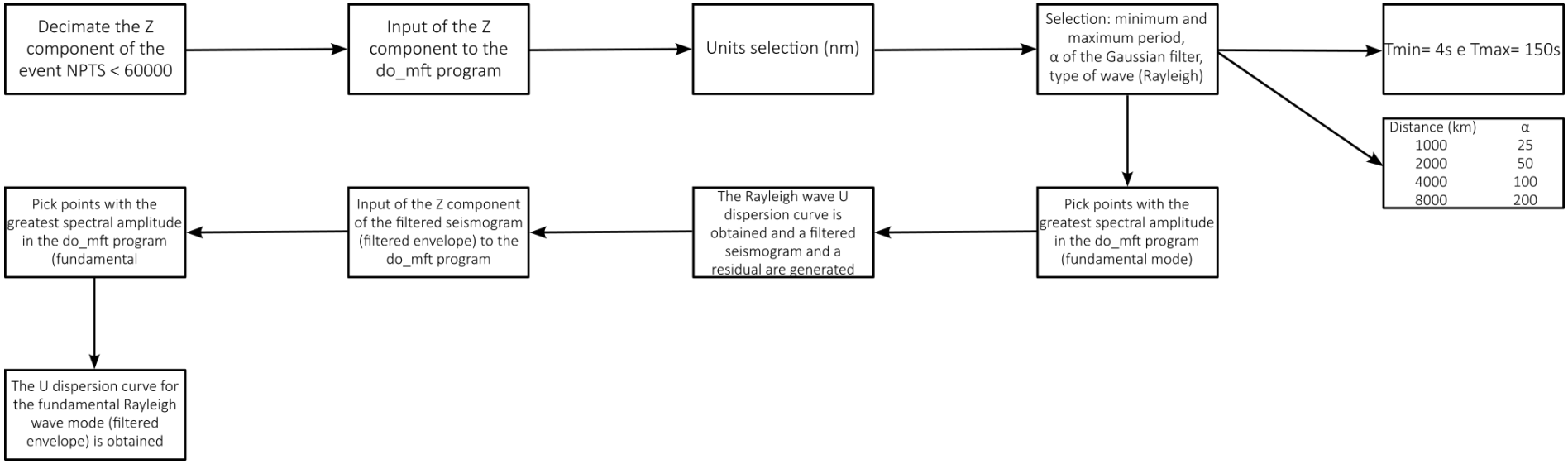

Figure 12: Processing phase of seismic event. The multiple filtering technique was performed with the do_mft program included in CPS: Computer Programs in Seismology (Herrmann, 2013). P-wave radial receiver functions that have reached the visual inspection phase are those that reproduced more than 85% of the signal after iterative deconvolution.

3.4. Joint Inversion

The steep angle of incidence presented by teleseismic P waves, used to calculate receiver functions, causes that S waves are mainly recorded in the horizontal components of seismograms (Ammon et al., 1990). Therefore, receiver functions are inverted to learn the S-wave velocity structure beneath a station (Owens, 1984). In addition, receiver functions are sensitive to velocity contrasts at interfaces, but contain very little information about the absolute velocity of S waves (Özalaybey et al., 1997). Ammon et al. (1990) pointed out that, when inverting the receiver functions to know the structure of shear rates, there is a velocity-depth trade-off that results in the non-uniqueness of the inversion of the receiver function.

On the other hand, surface wave dispersion is sensitive to the average shear velocity structure and for different periods they are able to sample structures at different depths. Therefore, they provide good information about the structure beneath a station in a rough manner, but are unable to provide information about discontinuities.

Therefore, several authors (Özalaybey et al., 1997; Julià et al., 2000, Herrmann & Ammon, 2002, among others) proposed inverting the data sets simultaneously, considering that both sample the same areas under one station and are sensitive to shear velocity. This allows finding a better determined velocity structure, with better constraints. The success of the joint inversion requires that both data sets be consistent and complementary (Julià et al., 2000), that is, that both sample the same portion of the propagation medium (the same part of the Earth) and provide constraints on the S wave velocity that improves those provided by each independent data set.

The joint inversion can be expressed in terms of the following equation (Herrmann & Ammon, 2002):

$$S = \frac{(1-p)}{N_r}\sum_{i=0}^{N_r}\left(\frac{O_{r_i} - P_{r_i}}{\sigma_{r_i}}\right)^2 + \frac{p}{N_s}\sum_{j=0}^{N_s}\left(\frac{O_{s_j} - P_{s_j}}{\sigma_{S_j}}\right)^2$$

We look for a velocity model that minimizes the functional S. Herrmann & Ammon (2002) pointed out that this equation is minimized by applying a singular value decomposition. In the functional S we have that, *O* refers to the observed data and *P* to

the predicted data; N_r and N_s represent the total number of observations of receiver function points and surface wave dispersion points, respectively; σ is the standard error; and p is the influence parameter which controls the relative influence of one dataset over the other, with $0 \leq p \leq 1$. p=0 means that the solution fits only the RF, while p=1 forces a solution based only on the dispersion.

We use the joint96 program from CPS (Herrmann, (2013) to perform the joint inversion with the first 60 seconds of the receiver functions and regionalized group dispersion observations for a period range of 8 – 150 seconds. The initial model is similar to the initial default model available in the CPS package. We modified only the crust of the default model, using 1 km thickness for the 10 shallowest layers., The Vp/Vs ratio (fixed in each layer) in the crust was set equal to that obtained by *H-k* stacking. The rest of the parameters of the initial model are the same as those of the model provided by the CPS package. An influence parameter of p=0.3 was used in this work, 30 iterations were performed during the joint inversion and a 0.5 damping value was established. Also, joint96 program allows adding smoothing to each individual layer, which we use for all layers of crust and upper mantle.

4. Submitted paper

The manuscript “Crustal thicknesses in Uruguay from joint inversion of receiver functions and surface wave dispersion” was submitted on March 7, 2024 to the special issue “Advances in the Knowledge of Crust and Lithosphere in Latin America Through Geophysical Studies” of the Journal of South American Earth Sciences.

Crustal thicknesses in Uruguay from joint inversion of receiver functions and surface wave dispersion

Martín Rodríguez-Kacevas[1*], Marcelo Assumpção[1], Leda Sánchez[2], Meijian An[3], and Mei Feng[3]

[1] *Institute of Astronomy, Geophysics and Atmospheric Sciences, University of São Paulo, São Paulo, Brasil*

[2] *Observatorio Geofísico de Uruguay, Facultad de Ciencias, Universidad de la República, Uruguay*

[3] *Chinese Academy of Geological Sciences, Beijing, China*

** Corresponding author: martinrodriguez@usp.br*

Abstract

The development of a seismic network in Uruguay in recent years has enabled studies of crustal structure in a region with few seismological studies of this type. In this work, we update the crustal thicknesses and Vp/Vs ratios calculated by H-k stack and present S-wave velocity models based on joint inversion of receiver functions and Rayleigh wave group velocity dispersion curves.

Some interesting results are the presence of a lower crust with a high S-wave velocity of 4.1 km/s below one of the stations located on the Río de la Plata Craton and the existence of a transitional Moho in Uruguay's northernmost station on the Paraná Basin, perhaps suggesting the presence of localized underplated material. A relatively thick crust, 41.8 km, compared to surrounding stations, was found beneath the Sierra Ballena Shear Zone in the Dom Feliciano Belt. We confirm the decrease in crustal thickness when approaching the oceanic coast, reaching a Moho depth of 36.3 km in SE Uruguay. Finally, the calculated Poisson's ratio allows inferring a crust of felsic to intermediate composition beneath most of Uruguay.

Introduction

The study of the structure of the crust using seismological techniques in Uruguay is very recent. Preliminary studies of receiver function and H-k stacking to estimate crustal thickness and Vp/Vs ratio were presented by Rodríguez et al. (2017; 2019). Later, Rivadeneyra-Vera et al. (2019), Rodríguez-Kacevas (2021), Rodríguez et al. (2022), presented more robust and accurate results using these techniques. Likewise, Castro Valle (2021) presented seismic Vp and Vs velocity models for the crust (up to 40 km depth approximately) for stations ANCO, PSAL, and TBOT (see Fig. 1 for location), through the inversion of Rayleigh-wave ellipticity curves using seismic noise and teleseisms.

Two broadband stations were installed in the last two years with a local project of the Geophysical Observatory of Uruguay (OGU) supported by CSIC (Comisión Sectorial de Investigación Científica, Universidad de la República).
In addition, two previous international collaborative projects allowed the installation of several broadband stations for relatively long periods: a) “3 Basins Project" (network XC), a collaboration project of the University of São Paulo (USP) in which UDELAR (Universidad de la República of Uruguay) participate, and b) collaboration project with CAGS (Chinese Academy of Geological Sciences). These projects focused on studying the crust in portions of southern Brazil, in parts of Paraguay, Argentina, Bolivia, and Uruguay. The main purpose of this study is to present S-wave velocity models of the crust and upper mantle for eight broadband stations in Uruguay (Fig. 1) using joint inversion of receiver function and surface wave dispersion observations. Additionally, updated estimates of crustal thickness, Vp/Vs ratio, and Poisson’s ratio calculations for these stations are also shown.

Geological Setting

Uruguay presents an important geological diversity. In a simplified way, the principal units are the Río de la Plata Craton in the southwestern sector of Uruguay, the southern portion of the Paraná Basin covering northern Uruguay, and finally, the Dom Feliciano Belt which comprises the southeastern sector of the country (Figure 1). Smaller features are also present inside or around these units, such as the Nico Perez Terrane (NPT),

which includes an Archaean block in central Uruguay, about which there is a debate regarding its belonging to the Río de la Plata Craton, and a small rotated block immersed in the Paraná Basin in northeastern Uruguay; and the Punta del Este Terrane (PET) in southeastern Uruguay, a unit with ages of 1.0 – 1.3 Ga in zircon xenocrysts (Hueck et al., 2018), and are interpreted as the basement rocks of the Dom Feliciano Belt.

Río de la Plata Craton

Río de la Plata Craton is the name that Almeida et al. (1973) gave to the Precambrian rocks outcropping in small sectors of eastern Argentina and southwestern Uruguay, the latter marking the eastern edge of the craton. However, most of this craton is covered by Phanerozoic sediments (Oyhantçabal et al., 2010; 2018 and references therein), with little geochronological evidence of it found to the west. An example of this is the U-Pb SHRIMP results from drilling samples in the Pampean mountains near Cordoba, which would mark the western edge of the craton (Rapela et al., 2007). There is no certainty about the northern extension of this craton; some authors propose that it could reach Paraguay but there is no definition on the subject.

Of interest in our study is the sector belonging to the southwest of Uruguay composed of Paleoproterozoic rocks, mainly an extensive area of granites, gneisses, and migmatites separated by metamorphic belts of supracrustal rocks (Sánchez Bettucci et al., 2010), locally called Piedra Alta Terrane (TPA) by Bossi et al. (1993).

Dom Feliciano Belt

The Neoproterozoic orogenic Dom Feliciano belt originated during the Brasiliano cycle, defined by Fragoso Cesar (1980), which extends along the Atlantic margin from southern Brazil to Uruguay. The portion of this belt found in Uruguay is divided into two domains separated by the Sierra Ballena Shear Zone (Oriolo et al., 2016; Hueck et al., 2018).

The western domain includes metavolcanic and metasedimentary rocks as well as basement inliers of the Nico Pérez Terrane (NPT in Fig. 1) and granitic intrusions, while the eastern domain includes the Punta del Este Terrane (PET) with some granitic intrusions such as the Santa Teresa granite (Hueck et al., 2018; Oyhantçabal et al., 2021).

Paraná Basin

The intracratonic Paraná basin extends for approximately 1.400.000 km^2 along southern Brazil, Argentina, Paraguay, and Uruguay, and has an approximately elliptical shape with an NNE - SSW trend. The origin of this basin occurs in the late Ordovician in the interior of Gondwana (Milani & Thomaz Filho, 2000). During the Mesozoic, one of the largest known episodes of basaltic magmatism was recorded related to the opening of the South Atlantic Ocean, known as the "Paraná Magmatic Province".

The southern sector of the Paraná Basin, in Uruguayan territory, is characterized by sedimentary deposits from the middle to upper Paleozoic covered by important basalt flows of Mesozoic age belonging to the Arapey Formation, interspersed with sandstones from the Tacuarembó Formation (Bossi, 1966), of Jurassic-Cretaceous age. These two formations are correlated with the Serra Geral Formation and the Botucatu Formation in Brazil, respectively.

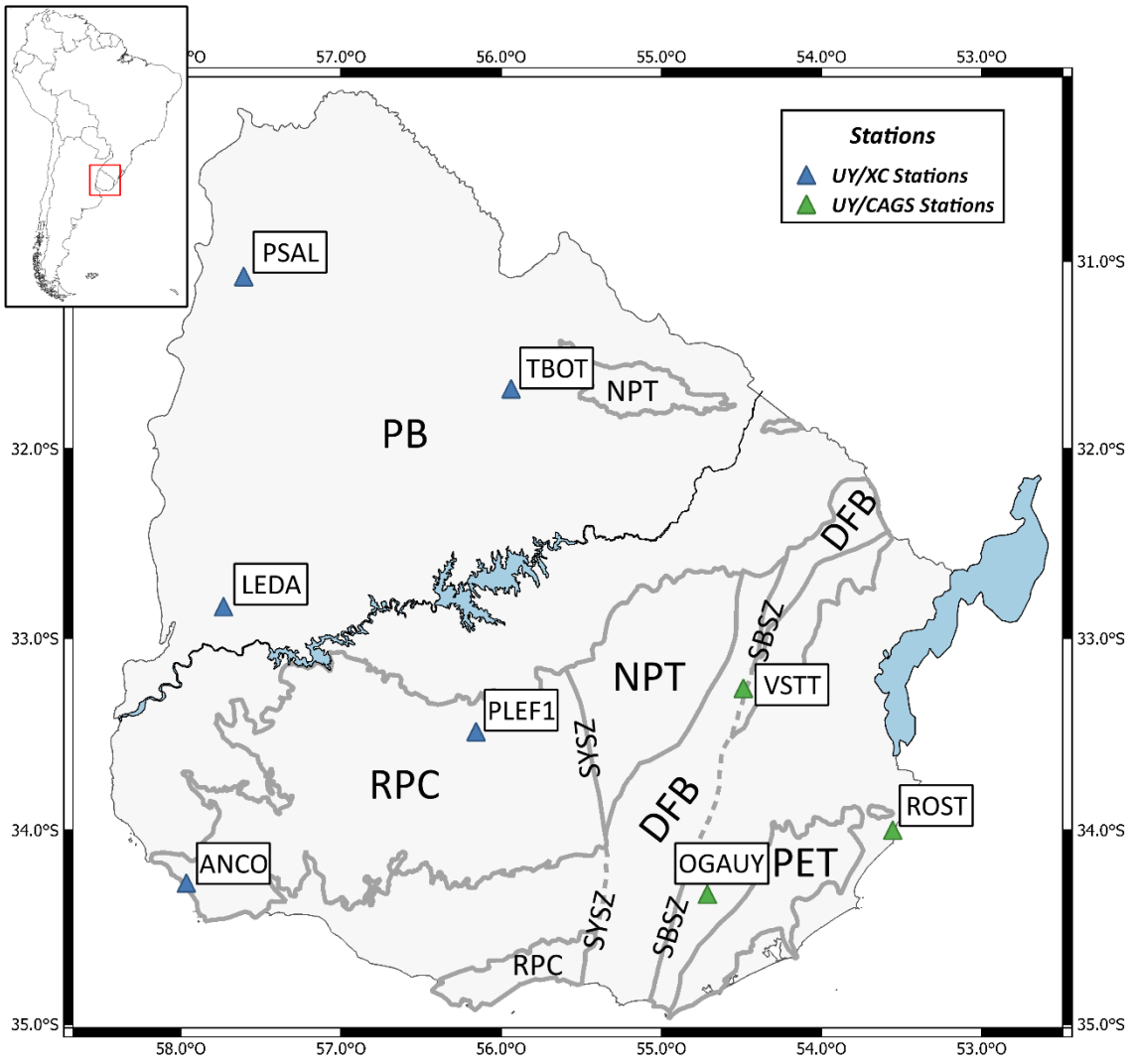

Figure 1: Simplified tectonic sketch of Uruguay (modified from Sánchez Bettucci et al., 2010; Hueck et al., 2018) showing the main tectonic units and also the broadband stations used in this study. PB: Paraná Basin; RPC: Río de la Plata Craton; DFB: Dom Feliciano Belt; NPT: Nico Pérez Terrane; PET: Punta del Este Terrane; SYSZ: Sarandí del Yí Shear Zone; SBSZ: Sierra Ballena Shear Zone.

Data, Methodology and Processing

The data used in this work come from broadband stations installed within the framework of various regional and international collaboration projects, as well as local projects of the Geophysical Observatory of Uruguay.

The eight broadband stations (Table 1) operated for different periods, generating an unequal dataset, with several years of data in some stations and in others barely exceeding one year of recording. Therefore, the results from some stations are more robust than others.

Station	Latitude	Longitude	Elevation (m)	H (km)	Vp/Vs (k)	σ	N
ANCO	-34.275	-57.965	252	40.8 ± 0.6	1.75 ± 0.02	0.26	59
LEDA	-32.834	-57.733	171	37.2 ± 4.2	1.85 ± 0.08	0.29	18
OGAUY	-34.333	-54.712	30	37.2 ± 3.1	1.75 ± 0.06	0.26	12
PLEF1	-33.489	-56.156	49	38.0 ± 0.9	1.73 ± 0.03	0.25	19
PSAL	-31.082	-57.607	15	42.2 ± 2.1	1.74 ± 0.04	0.25	70
ROST	-34.001	-53.554	62	36.3 ± 0.4	1.73 ± 0.02	0.25	8
TBOT	-31.682	-55.937	103	41.3 ± 3.1	1.77 ± 0.06	0.27	27
VSTT	-33.262	-54.487	54	41.8 ± 1.0	1.74 ± 0.03	0.25	21

Table 1: Summary of the main results from the broadband stations used in this research. Crustal thickness (H), Vp/Vs(k), and Poisson's ratio (σ) from H-k stacking.

Receiver Function

To know the structure of the crust and the upper mantle beneath a single seismological station, one of the most widespread techniques is the receiver function method (e.g. Burdick & Langston, 1977; Langston, 1979). This technique uses the fact that when a teleseismic P wave hits the base of the crust, a P to S converted wave ("Ps") will be generated and will arrive a few seconds after the direct P. This time difference between direct P and Ps can be used to estimate the depth of the discontinuity that generated the Ps phase. From a mathematical perspective, a receiver function is a time series that convolved with the vertical component of a seismogram, reproduces the horizontal components of the seismogram (Langston, 1977; Ligorría & Ammon, 1999). There are several procedures to deconvolve the vertical component from the radial (or tangential) component.

Two types of events were selected to generate the receiver functions: teleseismic events with 30° ≤ Δ ≤ 95° and magnitude above 6, and events deeper than 500km, magnitudes above 5, and Δ < 30°, removing the events coming from the triplication range. During the preprocessing stage, the events were visually inspected, detrended, and a taper was applied and then filtered between 0.05 and 10 Hz. Then, the P wave was picked and the events were cut from 10 seconds before the P arrival until 120 seconds in the case of teleseisms, and up to 60 seconds in the case of deep regional events. Finally, the traces were rotated to the ZRT components.

RF traces were generated using the iterative deconvolution in the time domain technique (Ligorría & Ammon, 1999) with 500 iterations. A Gaussian filter width of 2 was used for all stations. We selected only RFs with at least 85% reproduction of the original radial component.

Receiver functions are plotted, according to ray parameter and backazimuth, for station ANCO in Figure 2 (plots for the other stations are shown in the Supplementary Material). The direct P wave and Ps phase are clearly identified for all backazimuths and ray parameters. Besides the Moho-converted Ps phase, other reverberations are also recorded, such as the PpPs (P reflected at the surface and converted to S upon reflecting at the Moho), and PpSs+PsPs (different conversions at the surface and at the Moho with two crustal branches as S waves). These PpPs and PpSs+PsPs reverberations (or "multiples") are not as clear as the direct P wave and Ps phase, but can be identified in certain ranges of backazimuth and ray parameter, as shown in Fig. 2. These multiple phases can be enhanced by stacking techniques, as shown in Fig. 3. Because the move-out (variation of arrival time with distance) is different for each of the Ps and the two multiples, stacking was carried out separately for each of the converted phases. The stacked traces show the multiply reflected phases more clearly.

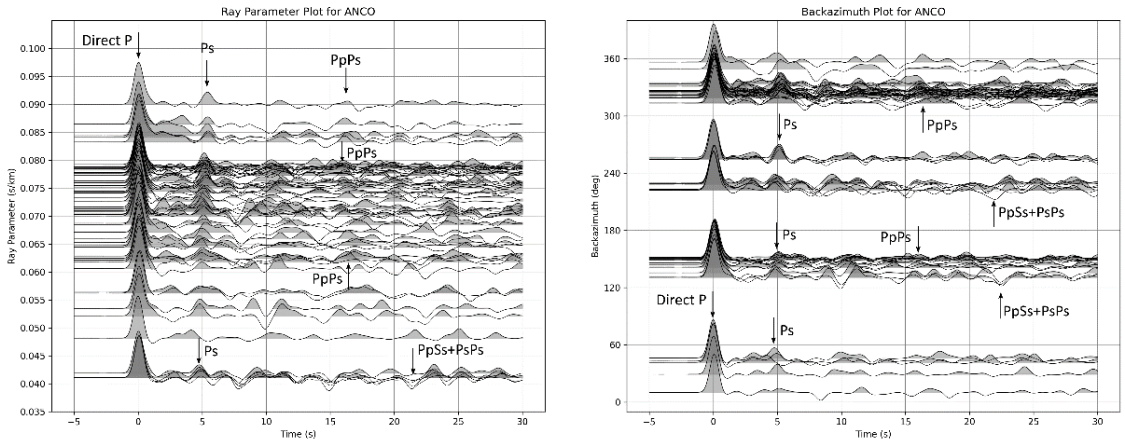

Figure 2: Plots of receiver functions versus ray parameter and backazimuth for station ANCO. Direct P-wave and Ps phase is identified for the entire range of backazimuths and ray parameters. PpPs phase is seen clearly in the backazimuths range of 310° – 330° and 125° – 150°. The second multiple is recognized with clarity for a ray parameter of approximately 0.040 and in various backazimuth ranges such as 125°, 210° – 250° and 315° – 330°.

H-k stacking

Zhu & Kanamori (2000) proposed a stacking algorithm for receiver functions that allows estimating crustal thickness (H) and Vp/Vs (k) ratio. It uses the amplitudes of the Ps as well as the multiply reflected, PpPs and PpSs+PsPs, to mitigate the trade-off between crustal thickness and Vp/Vs estimated only from the time difference between direct P and Ps. It consists of adding the amplitudes of the receiver functions at the predicted arrival times for the three phases for different H and k. The technique performs a grid search to find the H-k values that produce the largest stacked amplitude of Ps and the reverberations.

For the *H-k* stacking, we use this traditional method of Zhu & Kanamori (2000). An average crustal Vp=6.4 km/s was assumed, the weights of the Ps and the reverberations used were w_1=0.7 for the Ps phase, w_2=0.2 for the first multiple PpPs, and w_3=0.1 for the second multiple PpSs+PsPs. 200 bootstrap resamples (Efron & Tibshirani, 1991) were used to calculate the uncertainties in H and k.

Fig. 4 shows the results for the crustal thickness (*H*) and Vp/Vs ratio (*k*), summarized previously in Table 1. The stations in the Río de la Plata Craton (ANCO and PLEF1) show

a normal crust with a thickness close to 38 – 40 km and low uncertainties. The stations in the Dom Feliciano Belt presented more variability in thickness, with a station in the central part of the belt (VSTT) presenting a thickness close to 42 km, and the stations near the coast (OGAUY) showing significantly smaller thickness of 37 km. The three stations of the Paraná Basin presented larger thicknesses to the north 41 – 42 km (TBOT and PSAL), and to the south a thinner crust close to 37 km (LEDA) but with a large uncertainty (Figure 4). All Vp/Vs values were found to be in the average range of 1.73 to 1.77, except for LEDA, in the Paraná Basin, which has a high value of 1.85, but with a large uncertainty.

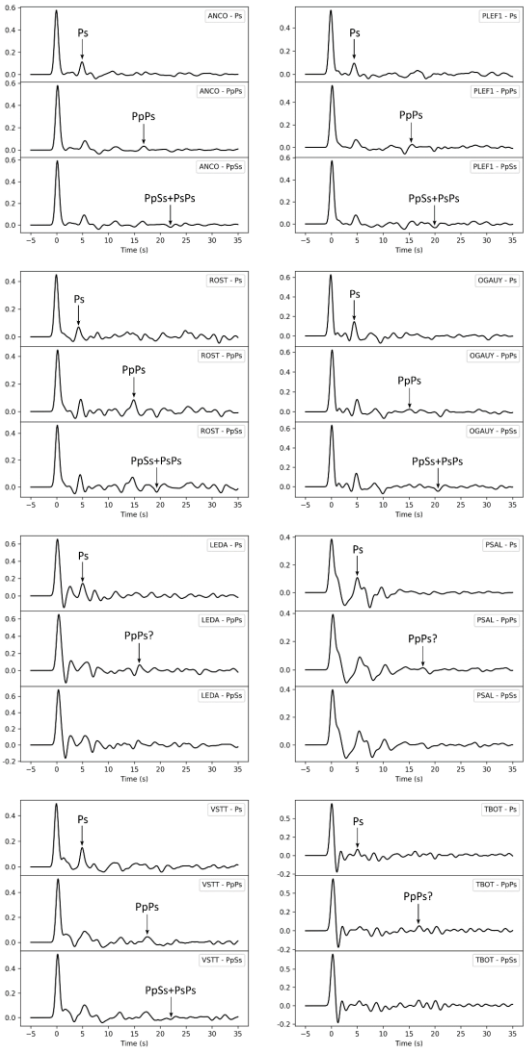

Figure 3: Stacked traces of P wave radial receiver functions using a Gaussian filter width α=2 after a moveout correction was applied for each phase (Ps, PpPs, and PpSs+PsPs) using a reference ray parameter p=0.06 s/km. Receiver function stacks in

stations LEDA and TBOT are noisier, probably due to the effect of the sedimentary layers below them.

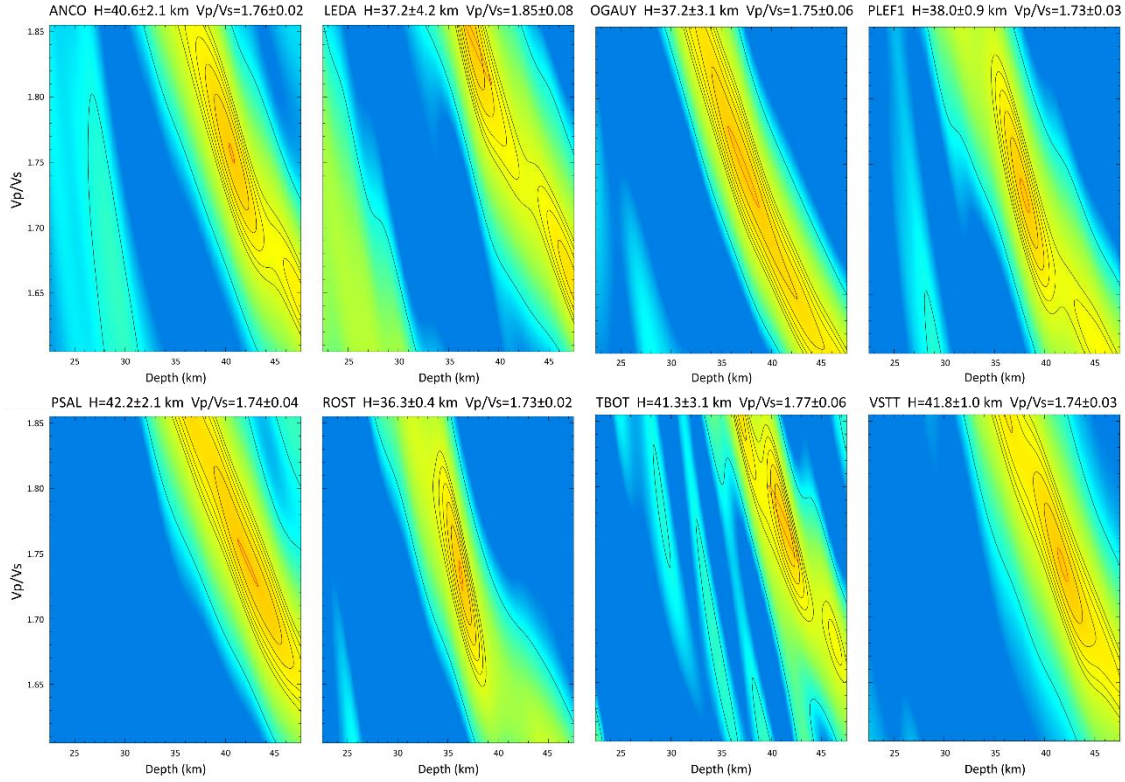

Figure 4: H-k stacking results for each station of this work.

Dispersion Curves

In this study, we calculated group velocity dispersion curves of Rayleigh surface waves for regional and teleseismic earthquakes using the multiple filtering technique, also known as MFT (Dziewonski et al., 1969; Herrin & Goforth, 1977), using the package "Computer Programs in Seismology (CPS)" (Herrmann, 2013).

We calculated group-velocity dispersion curves between the Uruguayan stations and earthquakes of magnitude ≥ 5.5 and Δ ≤ 45°, and therefore came mainly from the Andes and the South Sandwich Islands region. The instrumental response was removed in the frequency range of 0.007 to 0.3 Hz. A period range between 4 and 150 s was selected and a Gaussian filter width (α) was chosen for each event according to the epicentral-distance following the suggestion of Herrmann (2013). Then, the dispersion points corresponding to the maximum values of the envelope for the Rayleigh wave fundamental mode were picked. The resulting trace was filtered again with the phase-

matched filter to isolate the fundamental mode from other phases, yielding a cleaner group velocity dispersion curve.

Each station contributed with 15 to 120 dispersion curves, depending on recording time, and was used in a tomography model of SE South America by Moura et al. (2024). The regionalized dispersion curves at each Uruguayan station were used in a joint inversion with receiver functions.

Joint Inversion for S-wave velocity profile.

Julià et al. (2000) implemented a method to jointly invert P-wave receiver functions and surface wave dispersion curves to consistently estimate crustal and upper mantle structure. The method uses two independent data sets that individually constrain different aspects of the S-wave profile. Surface wave dispersion helps constrain the average absolute velocity of S-waves, while receiver functions better constrain small-scale velocity discontinuities (Julià et al., 2000).

The joint inversion can be expressed in terms of the following equation (Herrmann & Ammon, 2002):

$$S = \frac{(1-p)}{N_r}\sum_{i=0}^{N_r}\left(\frac{O_{r_i} - P_{r_i}}{\sigma_{r_i}}\right)^2 + \frac{p}{N_s}\sum_{j=0}^{N_s}\left(\frac{O_{s_j} - P_{s_j}}{\sigma_{s_j}}\right)^2$$

We look for a velocity model that minimizes the functional S, where: *O* refers to the observed data and *P* to the predicted data; N_r and N_s represent the total number of observations of receiver function points and surface wave dispersion points, respectively; σ is the standard error; and p is the influence parameter which controls the relative influence of one dataset over the other, with $0 \leq p \leq 1$. p=0 means that the solution fits only the RF, while p=1 forces a solution based only on the dispersion. We use the joint96 program from CPS (Herrmann, 2013) to perform the joint inversion with the first 60 seconds of the receiver functions and regionalized group dispersion observations for a period range of 8 – 150 seconds. The initial model is similar to the initial default model available in the CPS package. We modified only the crust of the default model, using 1 km thickness for the 10 shallowest layers., The Vp/Vs ratio (fixed in each layer) in the crust was set equal to that obtained by *H-k* stacking. The rest of the

parameters of the initial model are the same as those of the model provided by the CPS package.

The final model is composed of 88 layers, distributed as follows from the surface: 10 layers 1 km thick, 20 layers of 2 km thickness, 10 layers 5 km thick and finally the remaining layers 10 km thick. We will show the first 80 km of the S-wave velocity model, as this is the portion of greatest interest for our work and where we have the best resolution. An influence parameter of p=0.3 was found by trial and error to be the best compromise between fitting the RFs and the dispersion curve, 30 iterations were performed during the joint inversion and a 0.5 damping value was established. Figures 5, 6 and 7 presents the results obtained for stations VSTT, ANCO and PSAL, respectively, showing two examples of receiver function fit, the regionalized Rayleigh wave group velocity dispersion curve fit and the resulting S-wave velocity model (plots for the joint inversion of the other stations are shown in the Supplementary Material).

Finally, figure 8 shows a map with the stations, the main tectonic units, the S-wave velocity models and the *H-k* results for each station. In general, there is good agreement in the Moho depth calculated by both methods, with except for results from LEDA station.

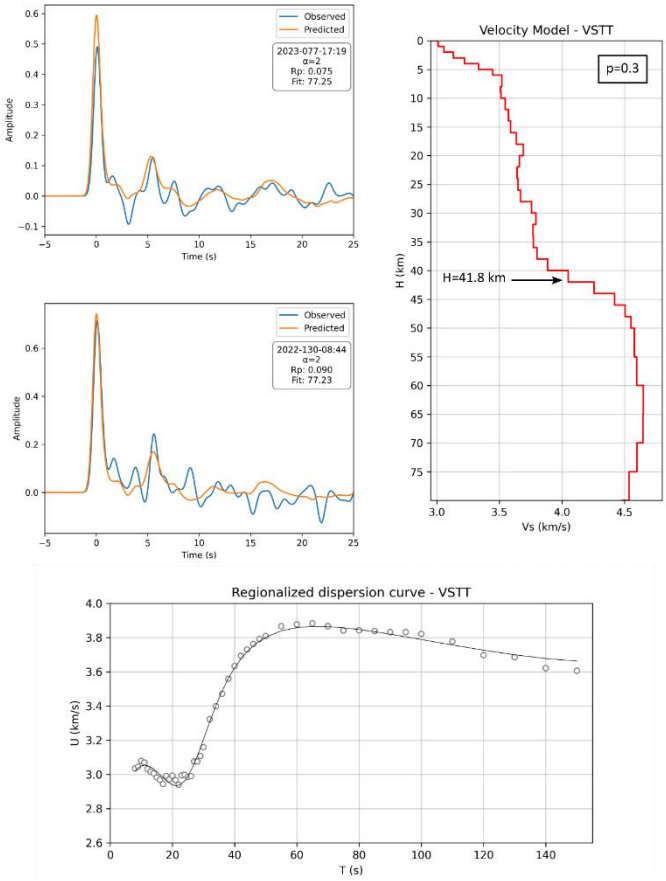

Figure 5: Joint inversion results for station VSTT. Examples of two observed (light blue line) and predicted (orange line) receiver functions fit (top). Observed (circles) and predicted (black line) regionalized Rayleigh group velocity dispersion curve (bottom). S wave velocity model obtained from the joint inversion (right), the black arrow indicates the Moho calculated by H-k stack.

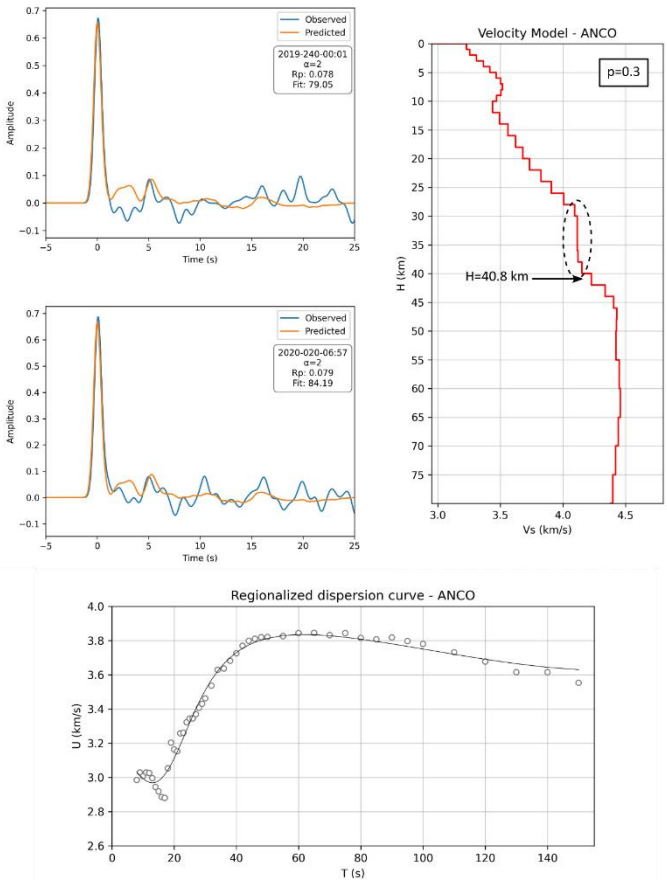

Figure 6: Joint inversion results for station ANCO. Examples of two observed (light blue line) and predicted (orange line) receiver functions fit (top). Observed (circles) and predicted (black line) regionalized Rayleigh group velocity dispersion curve (bottom). S wave velocity model obtained from the joint inversion (right). The black arrow indicates the Moho calculated by H-k stack and the dashed line ellipse marks the high velocity lower crust (≈4.1 km/s) under this station that could be interpreted as underplated material.

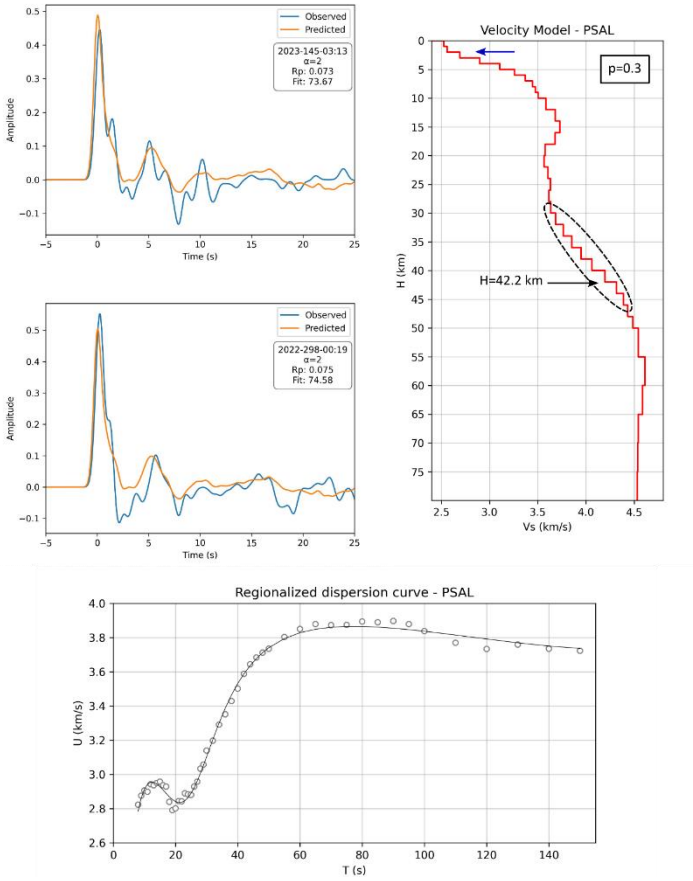

Figure 7: Joint inversion results for station PSAL. Examples of two observed (light blue line) and predicted (orange line) receiver functions fit (top). Observed (circles) and predicted (black line) regionalized Rayleigh group velocity dispersion curve (bottom). S wave velocity model obtained from the joint inversion (right). The black arrow indicates the Moho calculated by H-k stack and the dashed line ellipse marks the transitional Moho.

Discussion

Crustal Thickness and Vp/Vs ratio

Stations ANCO and PLEF1 located on the Río de la Plata Craton present receiver functions with a clear Ps and also recognizable reverberations in the stacks (Figure 3). Furthermore, these stations present average crust thicknesses, 40.6 km and 38.0 km, and with normal Vp/Vs values of 1.75 and 1.73 (Figure 4), respectively. These Vp/Vs values allow the Poisson's ratio to be calculated using:

$$\sigma = \frac{1}{2}\left\{1 - \left[\left(\frac{V_P}{V_S}\right)^2 - 1\right]^{-1}\right\}$$

The value of σ obtained for ANCO is 0.26, while for PLEF1 is 0.25. Following the work of Holbrook et al. (1992) and Zandt & Ammon (1995) we can note that these values indicate an average felsic composition for the crust of PLEF1, while an intermediate composition the crust beneath ANCO.

OGAUY, VSTT and ROST stations, located in the Dom Feliciano belt show crustal thicknesses that decrease as they approach the coast. This makes sense since it is expected that as we transition from continental crust to transitional crust (and oceanic crust) the depth of the Moho gets shallower.

ROST station, located practically on the east coast of Uruguay, is installed on the Early Cambrian Santa Teresa Granitic Complex, in the PET (Will et al., 2023), presents a robust H value of 36.3 km and a Vp/Vs of 1.73 despite the reduced number of receiver functions. These values are consistent with the Hk analysis of An et al. (2024), who found a crustal thickness of 36.7 ± 3.4 km e Vp/Vs 1.70 ± 0.3. OGAUY station presents a similar thin crust (37.2 km), although less constrained with a larger uncertainty of 3.1 km.

Another interesting case is VSTT station, which has a relatively thick crust of 41.8 km compared to the two previous stations. Also located in the DFB, this station has the peculiarity that it is located practically on an inferred (non-outcropping) sector of the Sierra Ballena shear zone (SBSZ). Therefore, it is plausible that this thickness is linked to this shear zone that separates the two domains of the DFB in Uruguay (Oriolo et al., 2016; Hueck et al., 2018). Moreover, a model for the DFB suggests that the collision that

created the belt was oblique and that the Major Gercino – Dorsal de Canguçu – Sierra Ballena Lineament is an old suture zone (Passarelli et al., 2011). This could explain the relatively thick crust. Regarding the Vp/Vs this station shows a standard value of 1.74.

Poisson's ratio for station ROST and VSTT is 0.25 which indicates an average felsic composition for the crust, while σ in OGAUY is 0.26 which suggest a more intermediate composition below this station.

Stations TBOT, PSAL and LEDA are located in the southern part of the Paraná basin. PSAL and TBOT show a normal to thick crust of 42.2 km and 41.3 km (Figure 4), respectively, similar to typical thicknesses of the Paraná basin in Brazil, mostly between 40 and 45 km (Rivadeneyra et al., 2019). Previous work by Rodríguez et al. (2017; 2019; 2022) and Rodríguez Kacevas (2021) reported crustal thicknesses similar to this for these stations. However, Rivadeneyra et al. (2019) show larger thicknesses of 44.4 ± 2.1 km and 45.4 ± 2.7 km for PSAL and TBOT, respectively. Furthermore, differences were also observed for the Vp/Vs values. Our study shows Vp/Vs ratios of 1.74 ± 0.04 and 1.77 ± 0.06 for PSAL and TBOT, respectively, while Rivadeneyra et al. (2019) showed values of 1.71 ± 0.05 and 1.70 ± 0.04. We identify two possible causes that may explain these differences: different event selection, accepted percentage of signal reproduction after deconvolution different in both works.

On the other hand, LEDA station, also in the Paraná basin, presents a thinner crust of 37.2 km and a Vp/Vs of 1.85, although the *H-k* stack result shows a second maximum 46 - 47 km and a Vp/Vs value of almost 1.65 (Figure 4). As a result, LEDA presents a large uncertainty in the calculated values of *H* and *Vp/Vs*, which may be due to the sedimentary structure beneath the station. Its stack (Figure 3) shows several peaks and troughs and only the Ps phase could be clearly identified but not the multiples. This fact also occurs in stations PSAL and TBOT where it is only possible to identify the first reverberation to a certain extent. Interference from converted waves inside the sedimentary basin could explain the less clear multiples in the three stations of the Paraná basin.

The Vp/Vs value of 1.85, despite its large uncertainty, is within the range of Vp/Vs found in continental regions (Zandt & Ammon, 1995; Zandt et al., 1995), while the value of

1.65 is already an extreme value, which makes the second maximum of the H-k stack less plausible.

Also, LEDA has only been in operation for a year so the number of receiver functions is low. Increasing the number of RFs and improving the azimuthal coverage would possibly decrease the uncertainty. More data will also allow to study if an inclined structure is present. Lack of good azimuthal coverage is a common problem in this region, since the vast majority of the receiver functions come from the azimuthal ranges of 145° – 160° (South Sandwich Islands) and 300° – 330° (Northern Andes and Central America) which prevents more detailed studies of dipping crustal layers or anisotropy.

Poisson's ratio of 0.25 for PSAL indicates a felsic composition for the crust, while for TBOT a value of 0.27 corresponding to a more intermediate composition. Finally, LEDA shows a Poisson's ratio of 0.29 which suggests a more mafic composition (presumably in the lower crust) although the Vp/Vs for this station has large uncertainties.

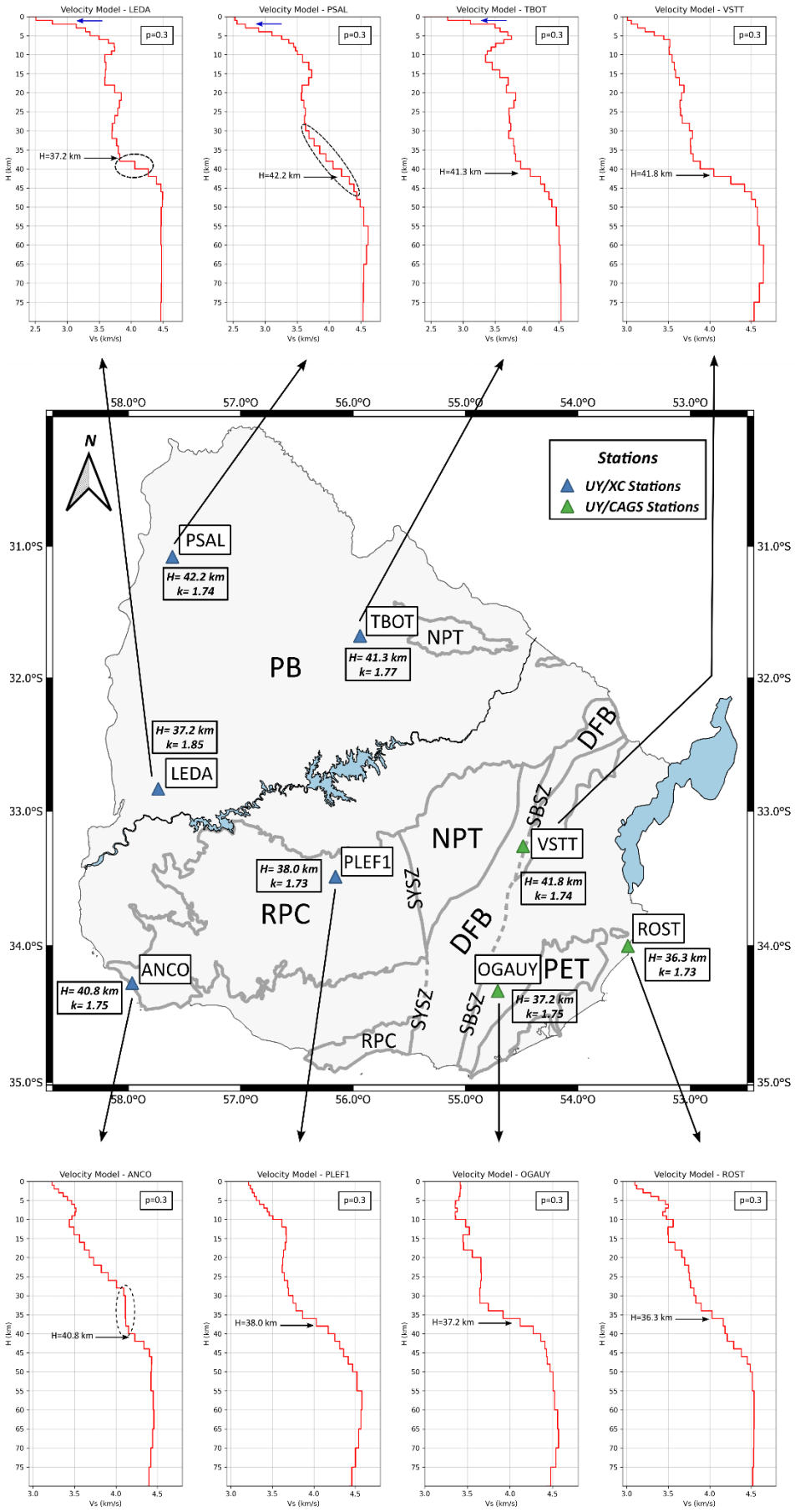
Velocity Model - LEDA
Velocity Model - PSAL
Velocity Model - TBOT
Velocity Model - VSTT
p=0.3
H=37.2 km
H=42.2 km
H=41.3 km
H=41.8 km
H (km)
Vs (km/s)
58.0°O
57.0°O
56.0°O
55.0°O
54.0°O
53.0°O
31.0°S
32.0°S
33.0°S
34.0°S
35.0°S
N
Stations
UY/XC Stations
UY/CAGS Stations
PSAL
H= 42.2 km
k= 1.74
TBOT
H= 41.3 km
k= 1.77
LEDA
H= 37.2 km
k= 1.85
PLEF1
H= 38.0 km
k= 1.73
VSTT
H= 41.8 km
k= 1.74
ROST
H= 36.3 km
k= 1.73
ANCO
H= 40.8 km
k= 1.75
OGAUY
H= 37.2 km
k= 1.75
PB
NPT
RPC
PET
DFB
SBSZ
SYSZ
Velocity Model - ANCO
Velocity Model - PLEF1
Velocity Model - OGAUY
Velocity Model - ROST

Figure 8: Summary map of Uruguay with main tectonic/geological units, broadband stations indicated by triangles, boxes that indicate crustal thickness and Vp/Vs (k) results from H-k stack and S wave velocity models for each station. In the S-wave velocity models, blue arrows indicate the inference of sedimentary rocks beneath the station, while black arrows mark the Moho depth calculated by H-k stacking, p indicate the influence parameter used for the joint inversion and dashed lined ellipses indicate a particular feature in the Vs model (more details in the text). PB: Paraná Basin; RPC: Río de la Plata Craton; DFB: Dom Feliciano Belt; NPT: Nico Pérez Terrane; PET: Punta del Este Terrane; SYSZ: Sarandí del Yí Shear Zone; SBSZ: Sierra Ballena Shear Zone.

S wave velocity profiles

Velocity models from stations PSAL, LEDA, and TBOT show low velocities less than 3.0 km/s in the first layers, indicated by the blue arrows in the Vs models of figure 8, consistent with their location in Paraná Basin.

In the case of LEDA, the model shows a low Vs of 2.5 km/s in the first layer, which should correspond to sedimentary rocks. However, independent information from the Ulleste drilling, located approximately 20 km NNW of LEDA, shows a layer of basalt and Paleozoic sediments below until reaching the basement at about 973 meters (Santa Ana et al., 2006). The basalt interspersed in the sediments would not justify Vs being so low in LEDA. The use of layers 1 km thick and FR with α= 2 does not allow the surface layers to be determined in detail. Another hypothesis is that the structure beneath the station is more sedimentary than sampled by the well, as it is located 20 km away and the geology can change greatly. Comparing the well data and our inversion there appears to be agreement, to some degree, that the basin has a thickness of about 1 km below this station, from which the basement begins.

Station PSAL exhibit a thicker sedimentary cover, or typically of this area interlayering of basalts and sedimentary rocks, evidenced by the first three layers with Vs velocities less than 2.7 km/s (Figure 7). In the Belen borehole, located approximately 25 km NNW of PSAL, the basement was found at a depth of 2330 m (Santa Ana et al., 2006), which is also consistent with our Vs model for this station. This drilling presents intercalation of basalts and sedimentary rocks.

TBOT presents the first layer with Vs 2.75 km/s corresponding to sedimentary rocks. The Tacuarembó and Bañado de Rocha drillings are located 10 km SSE and 25 km NE, respectively, of TBOT station. In the first drilling the basement is 350 meters deep, while in the second it is 702 meters deep (Santa Ana et al., 2006), which is to a certain extent consistent with our Vs model. Using thinner layers in the first kilometers of depth in the joint inversion could improve the resolution of the superficial sedimentary layer, but this would require recomputing the RFs with larger gaussian width to recover higher frequency content. It is important to point the absence of basaltic rocks in the two drillings.

A small discrepancy is observed between the depth of the Moho observed in the velocity model and that calculated by H-k stacking at the LEDA station (Figure 8). The Moho observed in the velocity model is somewhere between 38 and 42 km, plausibly near 40 km, while the H-k Moho is in 37.2 ± 4.2 km. However, these values are still within the uncertainties of each other.

An interesting feature is present in PSAL station. Contrary to all other stations which show a sharp Moho PSAL shows a transitional Moho from apparently 38 to 44 km of depth marked by the dashed line ellipse in figure 7. In fact, the RF stack from this station shows two consecutive peaks, the first one corresponding to the Moho, 5.1 seconds after de direct P wave approximately, and a second peak 1.2 seconds later (Figure 3), which can be an evidence to this transitional Moho. Additionally, a possible explanation to these peaks and the transitional Moho is that this feature corresponds to underplated material. Both peaks plausibly correspond to impedance contrasts of different magnitudes. The first one, being the largest in amplitude, as seen in the stack, could correspond to the contrast between the lower crust and the top of an underplated layer. The second peak of lower amplitude corresponding to the contrast between the underplated material and the upper mantle (i.e., the Moho). Julià et al. (2008) reported the presence of localized mafic underplating at select sites in the northern part of the Paraná Basin.

Stations on the Río de la Plata Craton show a very clear Moho that coincides with that found by *H-k* stack. The most interesting from these stations is the lower crust (≈28 to 40 km depth) of ANCO with a high Vs of approximately 4.1 km/s. Such high velocities in the lower crust are usually interpreted as underplating (Figure 6).

Conclusions

This work presents the first S wave velocity models for crust and upper mantle in Uruguay and also updates previous results from H-k stack, summarized in Figure 8.

Vs models corresponding to stations located in the Paraná basin show superficial sedimentary layers that are confirmed to some extent with independent information from nearby drillings.

Station ANCO, located on the Río de la Plata Craton, presents a lower crust with a high S wave velocity of approximately 4.1 km/s.

Stations located in SE Uruguay, a region corresponding mostly to DFB showed some variability in Moho depth, perhaps due to the fact that the stations are located in different domains of this belt.

Transitional Moho in under station PSAL located over the Paraná Basin, maybe suggesting the presence of localized underplated material or related to a local mafic magmatic phenomenon.

General agreement in Moho depth calculated by H-k stacking and joint inversion, with the exception of PSAL's transitional Moho and the disagreement showed in station LEDA, where crustal thickness of 37.2 km and Vp/Vs of 1.85 is calculated by H-k stack, but the Moho depth in the Vs model is nearer 40 km, although it must be considered that the H-k stack calculation has a great uncertainty.

Acknowledgements

This study was carried out with CAPES (Coordenação de Aperfeiçoamento de Pessoal de Nível Superior) M.Sc. Scholarship. We thank the "3-Basins Project Team" that participated in the generation of XC network dataset in Uruguay (Assumpção & Bianchi, 2016). We also thank Dr. Jordi Julià for providing the Hk Stack program.

References

Almeida, F.F.M., Amaral, G., Cordani, U.G., Kawashita, K. (1973). The Precambrian evolution of the South American cratonic margin, South of Amazonas River. In: Nairn ACM, Kanes WH, Stehli FG (eds) The Ocean Basins and Margins. Plenum, New York, pp 411–446.

An, M., Feng, M., Assumpção, M., Bianchi, M., França, G., Rocha, M., Sánchez Bettucci, L. (2024). Cratonic crust Interaction with Mantle Upwelling during Continental Rifting Implied from Vp/Vs beneath South America. Submitted to Geophysical journal international.

Assumpção, M. & Bianchi, M.B. (2016): Pantanal, Chaco and Paraná (PCPB) structural studies network. USP Seismological Center (USPSC). Dataset/Seismic Network. https://doi.org/10.7914/8scf-yd39

Bossi, J. (1966). Geología del Uruguay. Departamento de publicaciones de la Universidad de la República. Montevideo, Uruguay.

Bossi, J., Preciozzi, F. & Campal, N., (1993). Predevoniano en el Uruguay I: Terreno Piedra Alta. Dirección Nacional de Mineria y Geología, l: 1-50, Montevideo.

Burdick, L., & Langston, C.A. (1977). Modeling crustal structure through the use of converted phases in teleseismic body-wave forms. Bulletin of the Seismological Society of America.

Castro Valle, H. (2021). Inversión de la estructura de la corteza a través de curvas de elipticidad calculadas en base a ruido sísmico y telesismos. Tesis de grado. Montevideo: Udelar. FC.

Dziewonski A., Bloch S., Landisman M. (1969). A technique for analysis of transient seismic signals, Bull. Seism. Soc. Am., vol. 59, p. 427.

Efron, B., & Tibshirani, R. (1991). Statistical Data Analysis in the Computer Age. Science, 253(5018), 390-395.

Fragoso Cesar, A.R.S. (1980). O Cráton do rio de La Plata e o Cinturão Dom Feliciano no Escudo Uruguaio-Sul-Riograndense: XXXI Congresso Brasileiro de Geologia: Camboriú, v. 5, p. 2879–2892.

Herrin E., Goforth T. (1977). Phase-matched filters: Application to the study of Rayleigh waves, Bull. Seism. Soc. Am., vol. 67, p. 1259.

Herrmann, R.B. (2013). Computer programs in seismology: An evolving tool for instruction and research, Seism. Res. Lettr. 84, 1081-1088, doi:10.1785/0220110096.

Holbrook, W.S., Mooney, W.D., Christensen, N.I. (1992). In Continental Lower Crust (eds. Fountain, D. M., Arculus, R. & Kay, R.). 1-43 (El Sevier, Amsterdam).

Hueck, M., Oyhantçabal, P., Philipp, R.P., Basei, M.A.S., Siegesmund, S. (2018). The Dom Feliciano belt in southern Brazil and Uruguay. In: Siegesmund, S., Basei, M.A.S., Oyhantçabal, P., Oriolo, S. (Eds.), The Geology of Southwest Gondwana. Springer International Publishing, pp. 267–302.

Julià, J., Ammon, C. J., Herrmann, R. B., Correig, A. M. (2000). Joint inversion of receiver function and surface wave dispersion observations, Geophysical Journal International, Volume 143, Issue 1, October 2000, Pages 99–112, https://doi.org/10.1046/j.1365-246x.2000.00217.x

Julià, J., Assumpção, M., & Rocha, M. P. (2008). Deep crustal structure of the Paraná Basin from receiver functions and Rayleigh-wave dispersion: Evidence for a fragmented cratonic root, J. Geophys. Res., 113, B08318, doi:10.1029/2007JB005374.

Langston, C.A. (1977). Corvallis, Oregon, crustal and upper mantle structure from teleseismic P and S waves, Bull. Seism. Soc. Am. 67, 713-724.

Langston, C.A. (1979). Structure under Mount Rainier, Washington, inferred from teleseismic body waves, J. Geophys. Res. 84, 4749 – 4762.

Ligorría, J. & Ammon, C. (1999). Iterative deconvolution and receiver function estimation. Bulletin of Seismological Society of America, 89, 1395-1400.

Milani, E.J. & Thomaz Filho, A. (2000). Sedimentary basins of South America. In: Cordani, U.G., Milani, E. J., Thomaz Filho, A., Campos, D. A. (Ed.) Tectonic Evolution of South America. 31st IGC, Rio de Janeiro, Brazil, Special Publication, pp. 389 – 449.

Moura, D., Nascimento, A. Chaves, C. Marangoni, Y. & França, G. (2024). Lithospheric structure of the Paraná, Chaco-Paraná and Pantanal basins: insights from ambient noise and earthquake-based surface wave tomography. Submitted to Journal of South American Earth Sciences.

Oriolo, S., Oyhantçabal, P., Wemmer, K., Heidelbach, F., Pfänder, J., Basei, MAS., Hueck, M., Hannich, F., Sperner, B., Siegesmund, S. (2016). Shear zone evolution and timing of deformation in the Neoproterozoic transpressional Dom Feliciano Belt, Uruguay. J Struct Geol, 92:59–78.

Oyhantçabal, P., Siegesmund, S. & Wemmer, K. (2010). The Río de la Plata Craton: a review of units, boundaries, ages and isotopic signature. International Journal of Earth Sciences, 100: 20-35.

Oyhantçabal, P., Cingolani, C., Wemmer, K., Siegesmund, S. (2018). The Río de la Plata Craton of Argentina and Uruguay. In: Siegesmund, S., Basei, M.A.S., Oyhantçabal, P., Oriolo, S. (Eds.), The Geology of Southwest Gondwana. Springer International Publishing, pp. 267–302.

Oyhantçabal, P., Oriolo, S., Wemmer, K., Basei, M.A.S., Frei, D., Siegesmund S. (2021). Provenance of metasedimentary rocks of the western Dom Feliciano Belt in Uruguay: Insights from U–Pb detrital zircon geochronology, Hf and Nd model ages, and geochemical data, Journal of South American Earth Sciences, Volume 108, 103139, ISSN 0895-9811, https://doi.org/10.1016/j.jsames.2020.103139.

Passarelli, C.R., McReath, I., Basei, M.A.S., Siga, O.Jr., Campos Neto, M.C. (2011). Heterogeneity in syntectonic granitoids emplaced in a major shear zone, southern Brazil. Journal of South American Earth Sciences 32:369–378.

Rapela, C.W., Pankhurst, R.J., Casquet, C., Fanning, C.M., Baldo, E.G., González-Casado, J.M., Galindo, C., Dahlquist, J. (2007). The Río de la Plata Craton and the assembly of SW Gondwana. Earth-Sci Rev 83:49–82.

Rivadeneyra-Vera, C., Bianchi, M., Assumpção, M., Cedraz, V., Julià, J., Rodríguez, M., Sánchez, L., Sánchez, G., Lopez-Murua, L., Fernandez, G., Fugarazzo, R. & The "3-Basins" Project Team (2019). An updated crustal thickness map of central South America based on receiver function measurements in the region of the Chaco, Pantanal, and Paraná Basins, southwestern Brazil. Journal of Geophysical Research: Solid Earth, 124, 8491–8505. https://doi.org/10.1029/2018JB016811.

Rodríguez, M., Castro, H., Curbelo, A., Latorres, E., Castro Artola, O., Assumpção, M. y Sánchez Bettucci, L. (2017). Modelización 1D de la estructura de velocidades para la corteza en las cercanías a la localidad de Aiguá – Uruguay mediante inversión de función receptora. XXVIII Reunión Científica de la Asociación Argentina de Geofísica y Geodestas. Libro de Resúmenes, p. 246.

Rodríguez, M., Curbelo, A., Castro, H., Dell'Acqua, D., Latorres, E., Sánchez Bettucci, L. y Assumpção, M. (2019). Crustal thickness and Vp/Vs ratio for three stations in Uruguay using receiver function analysis: preliminary results. III Simpósio Brasileiro de Sismología.

Rodríguez Kacevas, M. (2021). Determinación del espesor cortical y la relación Vp/Vs debajo de tres estaciones sismológicas de banda ancha en Uruguay mediante el análisis de funciones receptoras [en línea] Tesis de grado. Montevideo: Udelar. FC.

Rodríguez, M., Sánchez Bettucci, L., Assumpção, M. (2022). Crustal thickness of Uruguay obtained by P-wave receiver functions. LACSC 4th Assembly Quito 2022. Abstr-062.

Sánchez Bettucci, L., Peel, E. & Oyhantçabal, P. (2010). Precambrian geotectonic units of the Río de la Plata craton. International Geology Review, 52: 1, 32 - 50.

Santa Ana, H., Veroslavsky, G., Fulfaro, V., Rossello, E. (2006). Capítulo VI: Cuenca Norte: evolución tectónica y sedimentaria del Carbonífero - Pérmico. In: Veroslavsky Barbe, G., Ubilla Gutiérrez, M. y Martínez Chiappara, S., (eds.). Cuencas sedimentarias de Uruguay: geología, paleontología y recursos naturales. Paleozoico [en línea] Montevideo: UR. FC. DIRAC, 2006.

Will, T.M., Gaucher, C., Frimmel, H.E., Ling, X.X., Shi, W., Li, X.H., & Li, Q.L. (2023). Ediacaran to Cambrian tectonomagmatic events in the Southern Dom Feliciano Belt, Uruguay: From a plate margin to an intraplate setting and the assembly of SW Gondwana. Gondwana Research, 115, 155-182.

Zandt, G., Myers, S. C., & Wallace, T. C. (1995). Crust and mantle structure across the Basin and Range-Colorado Plateau boundary at 37°N latitude and implications for Cenozoic extensional mechanism. Journal of Geophysical Research, 100(B6), 10,529–10,548. https://doi.org/10.1029/94jb03063.

Zandt, G. & Ammon, C. J. (1995). Continental crust composition constrained by measurements of crustal Poisson's ratio. Nature, 374(6518), 152-154. https://doi.org/10.1038/374152a0.

Zhu, L., & H. Kanamori (2000). Moho depth variation in southern California from teleseismic receiver functions, J. Geophys. Res., 105, 2969 – 2980.

5. Bibliography

Almeida, F.F.M., Amaral, G., Cordani, U.G., Kawashita, K. (1973). The Precambrian evolution of the South American cratonic margin, South of Amazonas River. In: Nairn ACM, Kanes WH, Stehli FG (eds) The Ocean Basins and Margins. Plenum, New York, pp 411–446.

Ammon, C. J., G. E. Randall, and G. Zandt (1990). On the nonuniqueness of receiver function inversions, J. Geophys. Res., 95, 15303-15318.

Ammon, C.J. (1991). The isolation of receiver effects from teleseismic P waveforms, Bull. Seism.Soc. Am. 81, 2504-2510.

Aster, R., Borchers, B., Thurber, C. (2012). Parameter Estimation and Inverse Problems. Recherche. 67. 02.

Castro Valle, H. (2021). Inversión de la estructura de la corteza a través de curvas de elipticidad calculadas en base a ruido sísmico y telesismos. Tesis de grado. Montevideo: Udelar. FC.

Cingolani, C.A. (2011). The Tandilia system of Argentina as southern extension of the Río de la Plata craton: an overview. Int J Earth Sci 100:221–242.

Dziewonski A., Bloch S., Landisman M. (1969). A technique for analysis of transient seismic signals, Bull. Seism. Soc. Am., vol. 59, p. 427.

Fragoso Cesar, A.R.S. (1980). O Cráton do rio de La Plata e o Cinturão Dom Feliciano no Escudo Uruguaio-Sul-Riograndense: XXXI Congresso Brasileiro de Geologia: Camboriú, v. 5, p. 2879–2892.

Goldstein, P., A. Snoke, (2005), “SAC Availability for the IRIS Community”, Incorporated Institutions for Seismology Data Management Center Electronic Newsletter.

Goldstein, P., D. Dodge, M. Firpo, Lee Minner (2003) “SAC2000: Signal processing and analysis tools for seismologists and engineers, Invited contribution to “The IASPEI International Handbook of Earthquake and Engineering Seismology”,

Edited by WHK Lee, H. Kanamori, P.C. Jennings, and C. Kisslinger, Academic Press, London.

Herrin E., Goforth T. (1977). Phase-matched filters: Application to the study of Rayleigh waves, Bull. Seism. Soc. Am., vol. 67, p. 1259.

Herrmann, R. B. and C. J., Ammon (2002). Computer program in seismology; surface waves, receiver functions, and crustal structure, Version 3.15, Saint Louis University.

Herrmann, R.B. (2013). Computer programs in seismology: An evolving tool for instruction and research, Seism. Res. Lettr. 84, 1081-1088, doi:10.1785/0220110096.

Hueck, M., Oyhantçabal, P., Philipp, R.P., Basei, M.A.S., Siegesmund, S. (2018). The Dom Feliciano belt in southern Brazil and Uruguay. In: Siegesmund, S., Basei, M.A.S., Oyhantçabal, P., Oriolo, S. (Eds.), The Geology of Southwest Gondwana. Springer International Publishing, pp. 267–302.

Julià, J., Ammon, C. J., Herrmann, R. B., Correig, A. M. (2000). Joint inversion of receiver function and surface wave dispersion observations, Geophysical Journal International, Volume 143, Issue 1, October 2000, Pages 99–112, https://doi.org/10.1046/j.1365-246x.2000.00217.x

Langston, C.A. (1977). Corvallis, Oregon, crustal and upper mantle structure from teleseismic P and S waves, Bull. Seism. Soc. Am. 67, 713-724.

Langston, C.A. (1979). Structure under Mount Rainier, Washington, inferred from teleseismic body waves, J. Geophys. Res. 84, 4749 – 4762.

Ligorría, J. & Ammon, C. (1999). Iterative deconvolution and receiver function estimation. Bulletin of Seismological Society of America, 89, 1395-1400.

Milani, E.J. & Thomaz Filho, A. (2000). Sedimentary basins of South America. In: Cordani, U.G., Milani, E. J., Thomaz Filho, A., Campos, D. A. (Ed.) Tectonic Evolution of South America. 31st IGC, Rio de Janeiro, Brazil, Special Publication, pp. 389 – 449.

Moura, D., Nascimento, A. Chaves, C. Marangoni, Y. & França, G. (2024). Lithospheric structure of the Paraná, Chaco-Paraná and Pantanal basins: insights from ambient noise and earthquake-based surface wave tomography. Submitted to Journal of South American Earth Sciences.

Muzio, R. (2004). Capítulo IV – El magmatismo mesozoico en Uruguay y sus recursos minerales. In: Veroslavsky Barbe, Gerardo, Ubilla Gutierrez, Martín y Martinez Chiappara, Sergio Agustín, (eds.). Cuencas sedimentarias de Uruguay: geología, paleontología y recursos naturales: Mesozoico [en línea] 2a. ed. Montevideo: UR. FC. DIRAC; SUG, 2004.

Oriolo, S., Oyhantçabal, P., Wemmer, K., Heidelbach, F., Pfänder, J., Basei, MAS., Hueck, M., Hannich, F., Sperner, B., Siegesmund, S. (2016). Shear zone evolution and timing of deformation in the Neoproterozoic transpressional Dom Feliciano Belt, Uruguay. J Struct Geol, 92:59–78.

Owens, T.J., Zandt, G. and Taylor, S.R. (1984). Seismic evidence for an ancient rift beneath the Cumberland Plateau, Tennessee: A detailed analysis of broadband teleseismic P waveforms, J. Geophys. Res., 89(B9), 7783–7795, doi:10.1029/JB089iB09p07783.

Oyhantçabal, P., Siegesmund, S. & Wemmer, K. (2011). The Río de la Plata Craton: a review of units, boundaries, ages and isotopic signature. International Journal of Earth Sciences, 100: 20-35.

Oyhantçabal, P., Cingolani, C., Wemmer, K., Siegesmund, S. (2018). The Río de la Plata Craton of Argentina and Uruguay. In: Siegesmund, S., Basei, M.A.S., Oyhantçabal, P., Oriolo, S. (Eds.), The Geology of Southwest Gondwana. Springer International Publishing, pp. 267–302.

Özalaybey, S., Savage, M.K., Sheehan, A.F., Louie, J.N. and Brune, J.N. (1997). Shear-wave velocity structure in the northern Basin and Range province from the combined analysis of receiver functions and surface waves, Bull. Seism. Soc. Am., 87, 183-199.

Peate, D.W. (1997). The Paraná-Etendeka Province, pp. 217-245 de Mahoney JJ & Coffin MF (eds.): Large igneous provinces, continental: oceanic and planetary flood volcanism. American Geophysical Union, Geophysical Monograph 100.

Rawlinson, N. & Sambridge M. (2005). "The fast-marching method: An effective tool for tomographic imaging and tracking multiple phases in complex layered media", Explor. Geophys., 36, 341-350.

Rivadeneyra-Vera, C., Bianchi, M., Assumpção, M., Cedraz, V., Julià, J., Rodríguez, M., Sánchez, L., Sánchez, G., Lopez-Murua, L., Fernandez, G., Fugarazzo, R. & The "3-Basins" Project Team (2019). An updated crustal thickness map of central South America based on receiver function measurements in the region of the Chaco, Pantanal, and Paraná Basins, southwestern Brazil. Journal of Geophysical Research: Solid Earth, 124, 8491–8505. https://doi.org/10.1029/2018JB016811.

Rodríguez, M., Castro, H., Curbelo, A., Latorres, E., Castro Artola, O., Assumpção, M. y Sánchez Bettucci, L. (2017). Modelización 1D de la estructura de velocidades para la corteza en las cercanías a la localidad de Aiguá – Uruguay mediante inversión de función receptora. XXVIII Reunión Científica de la Asociación Argentina de Geofísica y Geodestas. Libro de Resúmenes, p. 246.

Rodríguez, M., Curbelo, A., Castro, H., Dell'Acqua, D., Latorres, E., Sánchez Bettucci, L. y Assumpção, M. (2019). Crustal thickness and Vp/Vs ratio for three stations in Uruguay using receiver function analysis: preliminary results. III Simpósio Brasileiro de Sismología.

Rodríguez Kacevas, M. (2021). Determinación del espesor cortical y la relación Vp/Vs debajo de tres estaciones sismológicas de banda ancha en Uruguay mediante el análisis de funciones receptoras [en línea] Tesis de grado. Montevideo: Udelar. FC.

Rodríguez, M., Sánchez Bettucci, L., Assumpção, M. (2022). Crustal thickness of Uruguay obtained by P-wave receiver functions. LACSC 4th Assembly Quito 2022. Abstr-062.

Sánchez Bettucci, L., Peel, E. & Oyhantçabal, P. (2010). Precambrian geotectonic units of the Río de la Plata craton. International Geology Review, 52: 1, 32 - 50.

Santa Ana, H., Veroslavsky, G., Fulfaro, V., Rossello, E. (2006). Capítulo VI: Cuenca Norte: evolución tectónica y sedimentaria del Carbonífero - Pérmico. In: Veroslavsky Barbe, G., Ubilla Gutiérrez, M. y Martínez Chiappara, S., (eds.). Cuencas sedimentarias de Uruguay: geología, paleontología y recursos naturales. Paleozoico [en línea] Montevideo: UR. FC. DIRAC, 2006.

Zhu, L., & H. Kanamori (2000). Moho depth variation in southern California from teleseismic receiver functions, J. Geophys. Res., 105, 2969 – 2980.

6. Appendix

6.1. Data availability and quality control

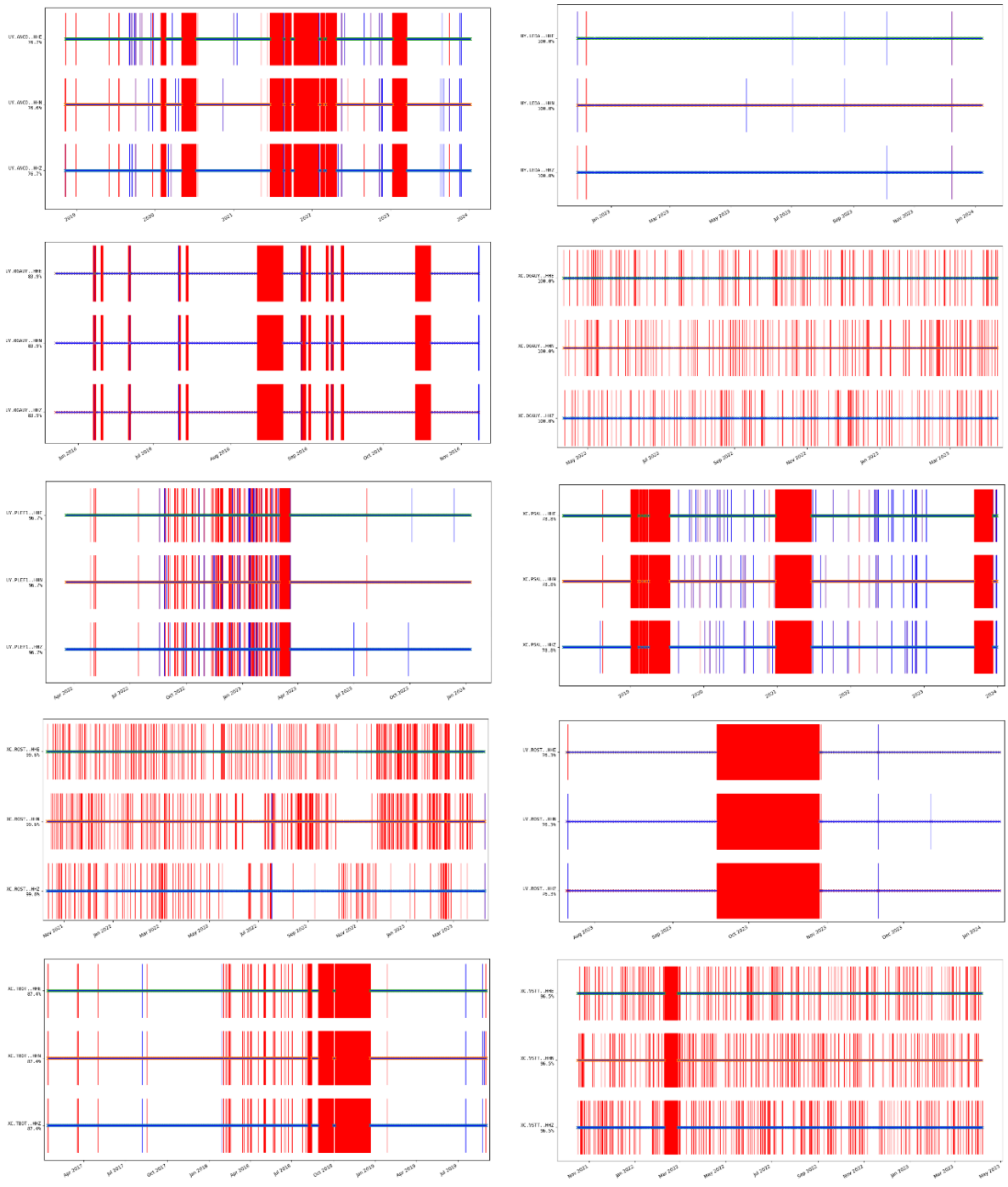

Figure 13: Data availability for each station in this research. The plots were carried out using obspy-scan plotting routine. Red lines indicate gaps while blue lines mark an overlap.

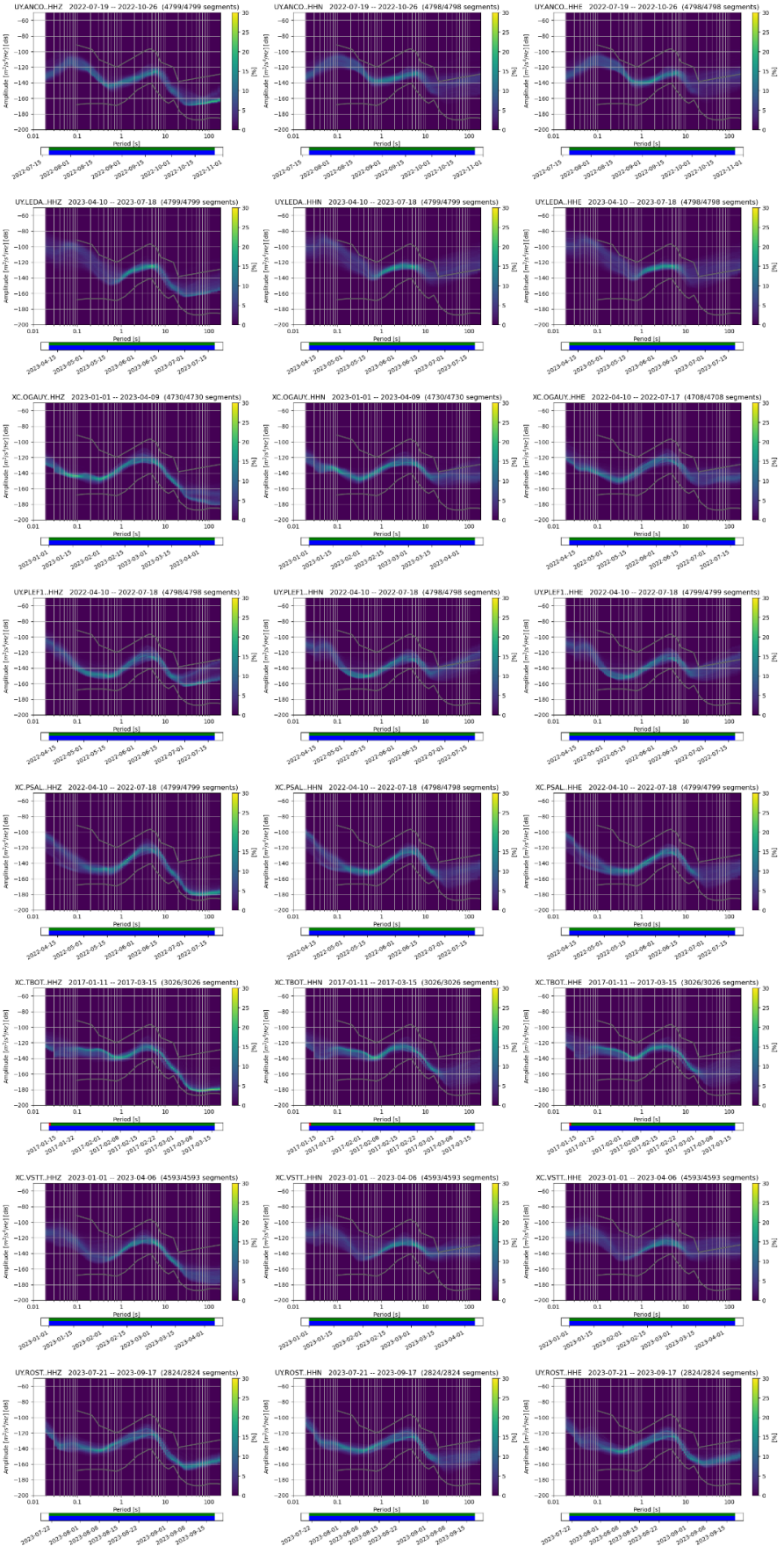

Figure 14: Noise curves for each of the stations in this study.

6.2. Borehole data

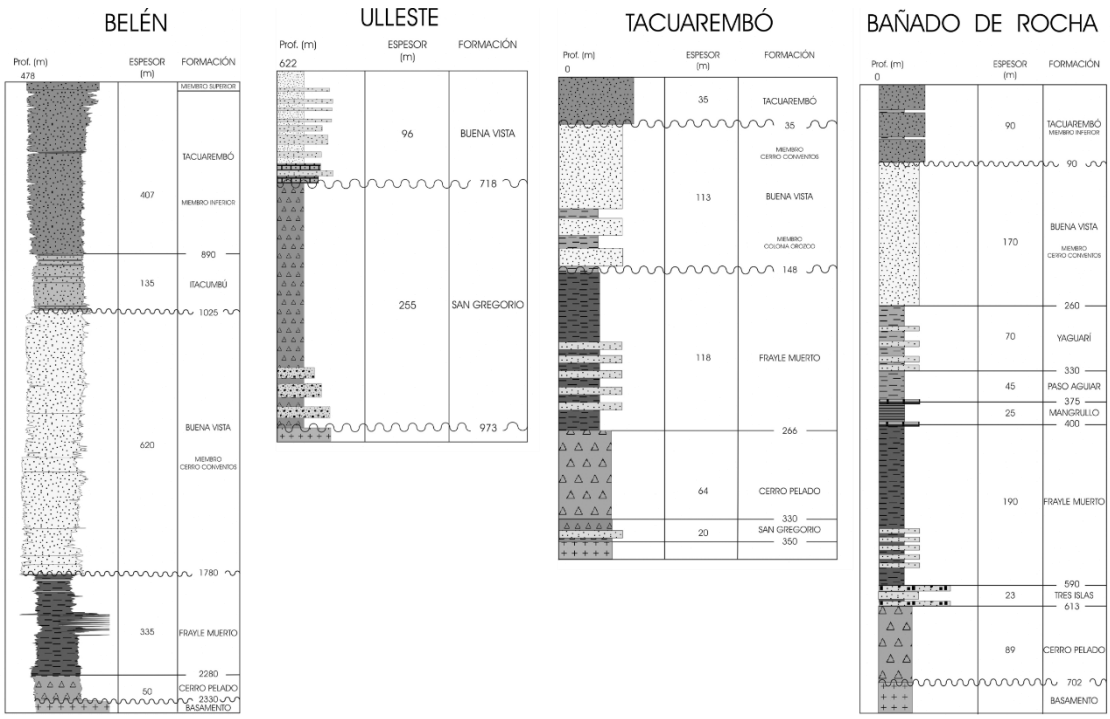

Figure 15: Borehole data (Taken from Santa Ana et al., 2006).

6.3. Supplementary material of submitted paper

Additional figures for the paper "Crustal thicknesses in Uruguay from joint inversion of receiver functions and surface wave dispersion" by Martín Rodríguez, Marcelo Assumpção Leda Sánchez, Meijian An and Mei Feng

List of supplementary material figures

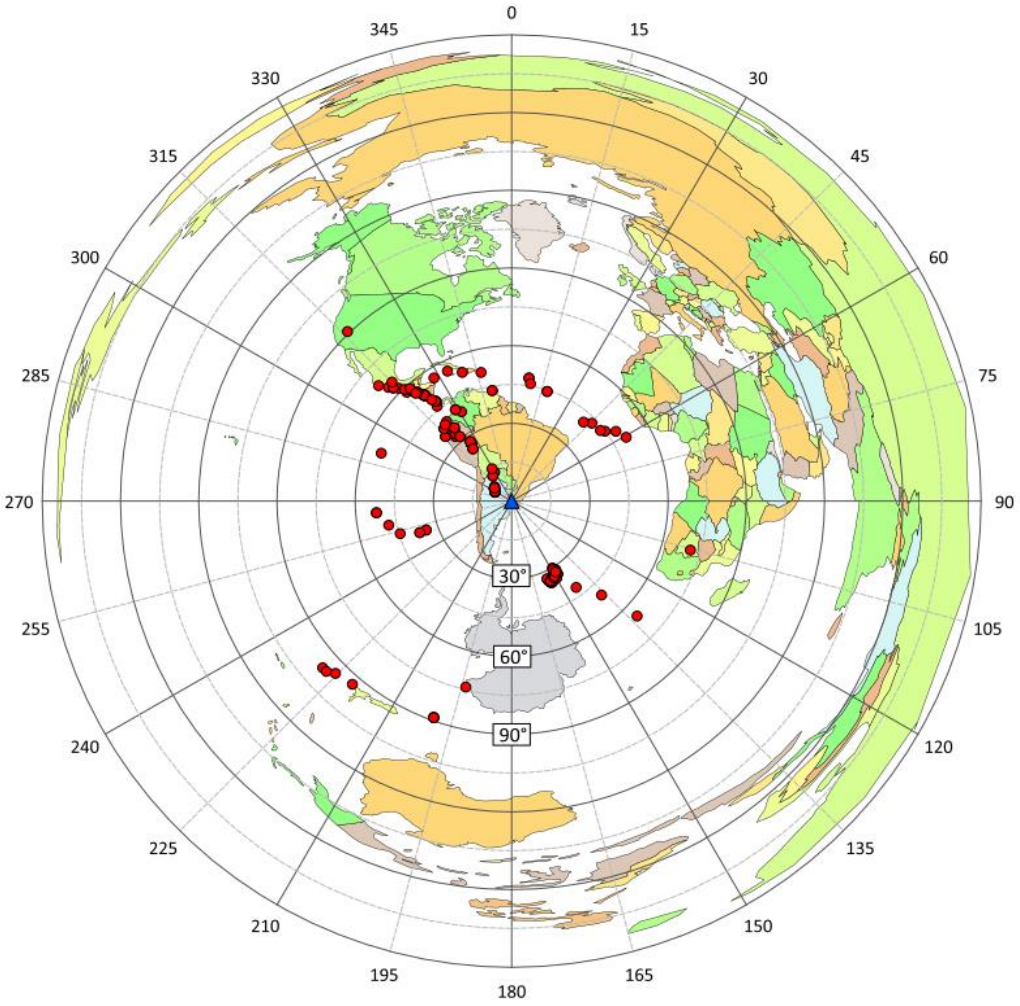

Figure S1: Distribution of earthquake epicenters used to apply the receiver function method.

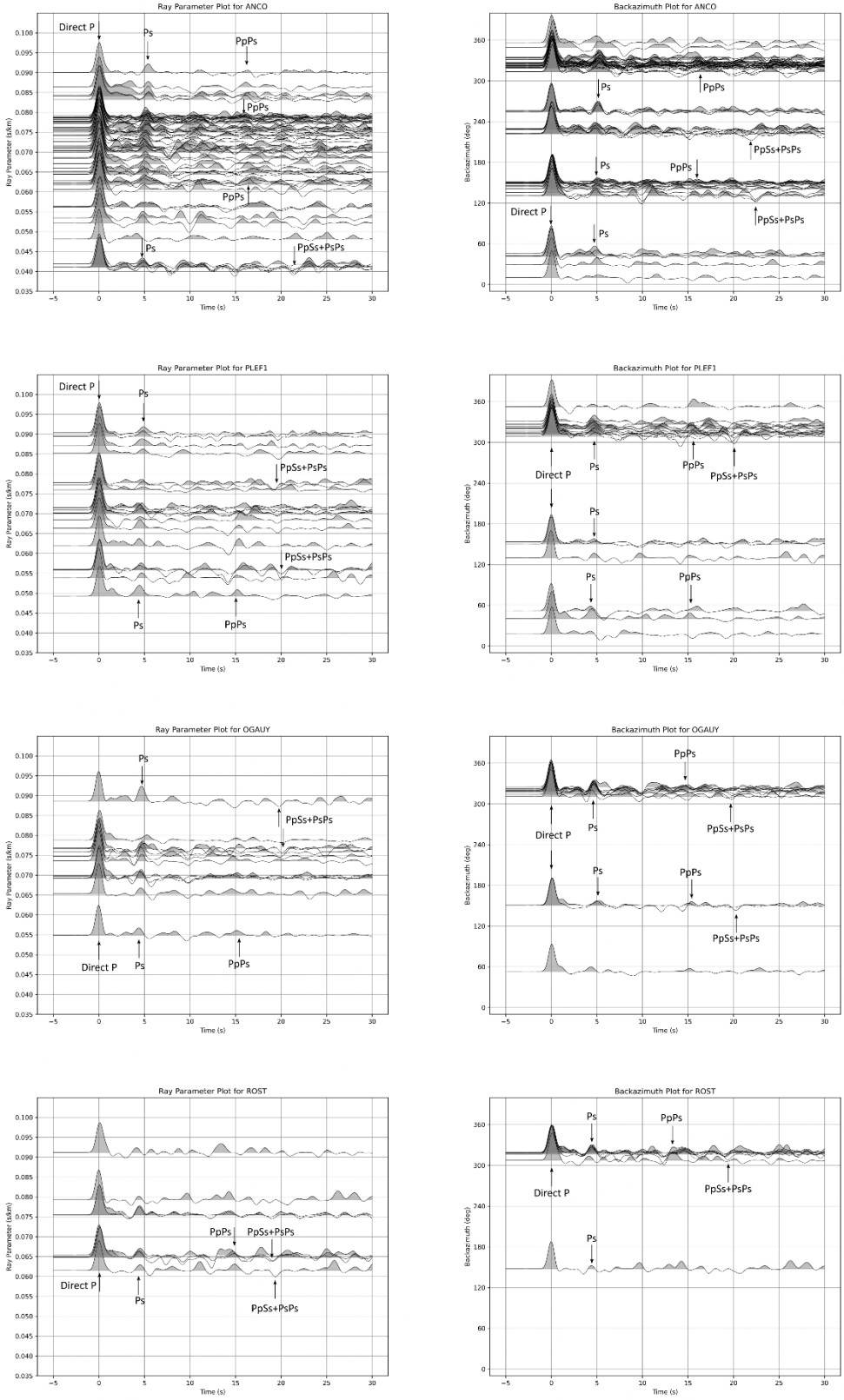

Figure S2: Receiver function plots for four stations, ordered by ray parameter and backazimuth marking the main phases present.

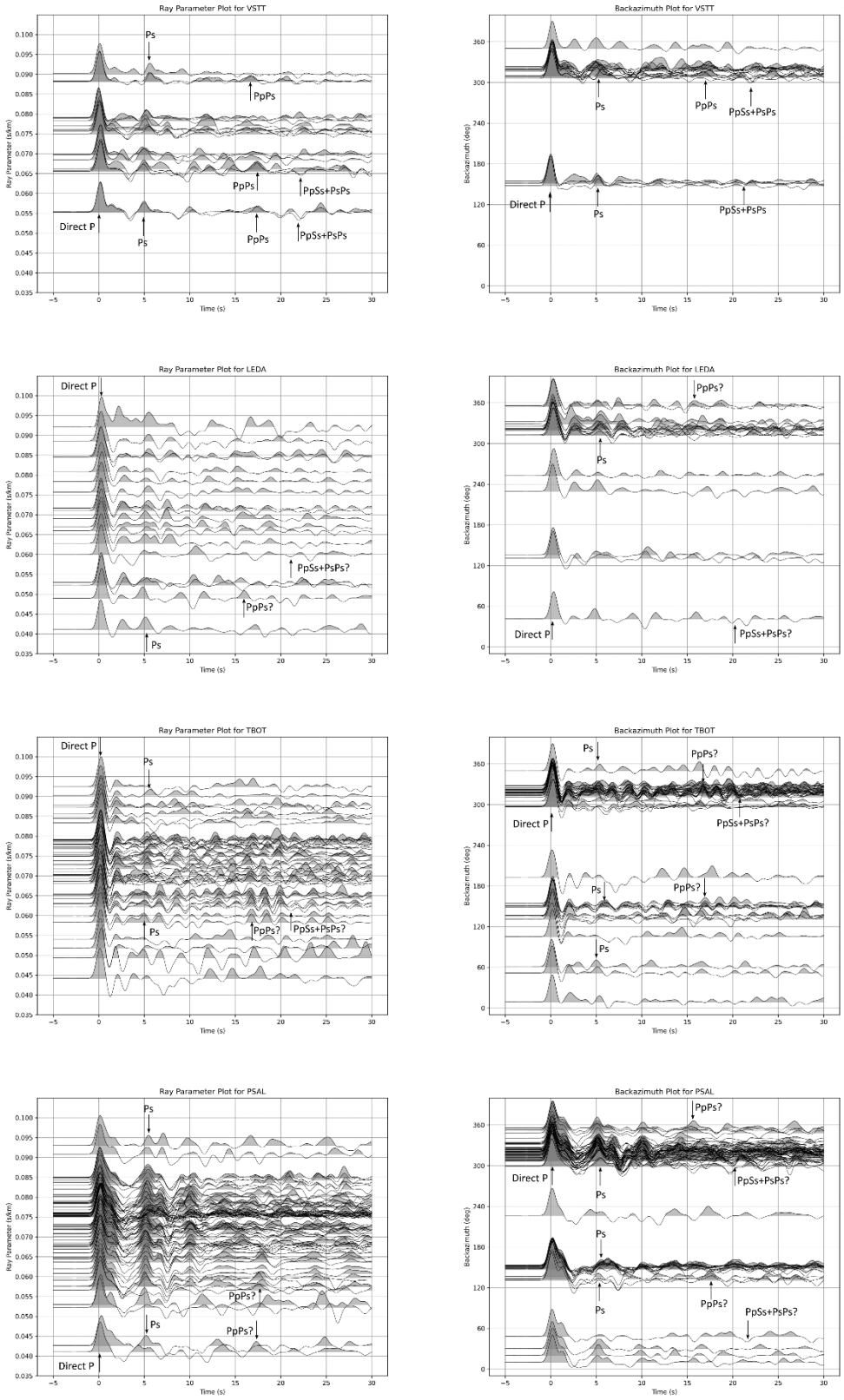

Figure S3: Receiver function plots for four stations, ordered by ray parameter and backazimuth marking the main phases present.

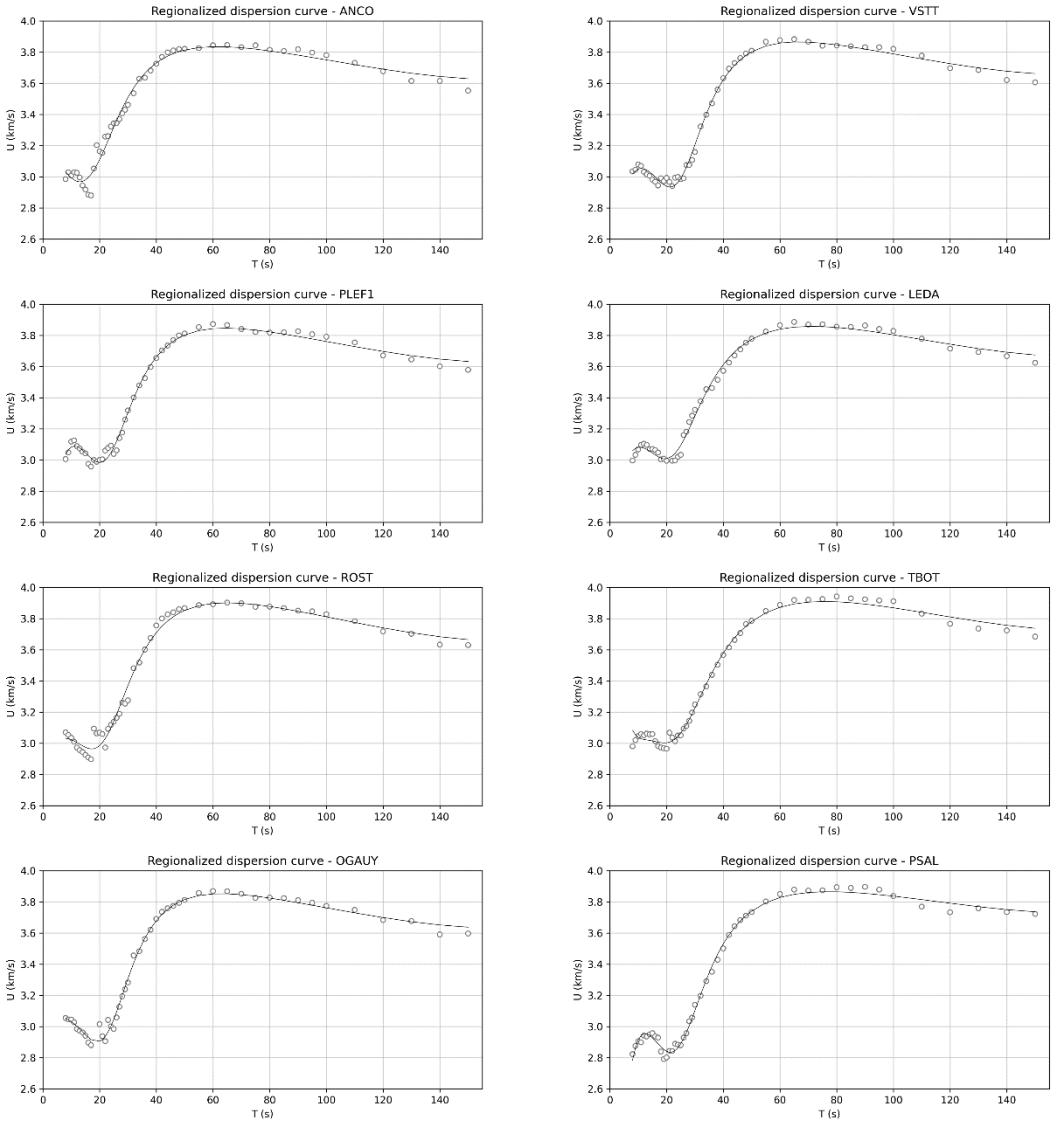

Figure S4: Observed (circles) and predicted (black line) Rayleigh wave dispersion curves for each station of this work.

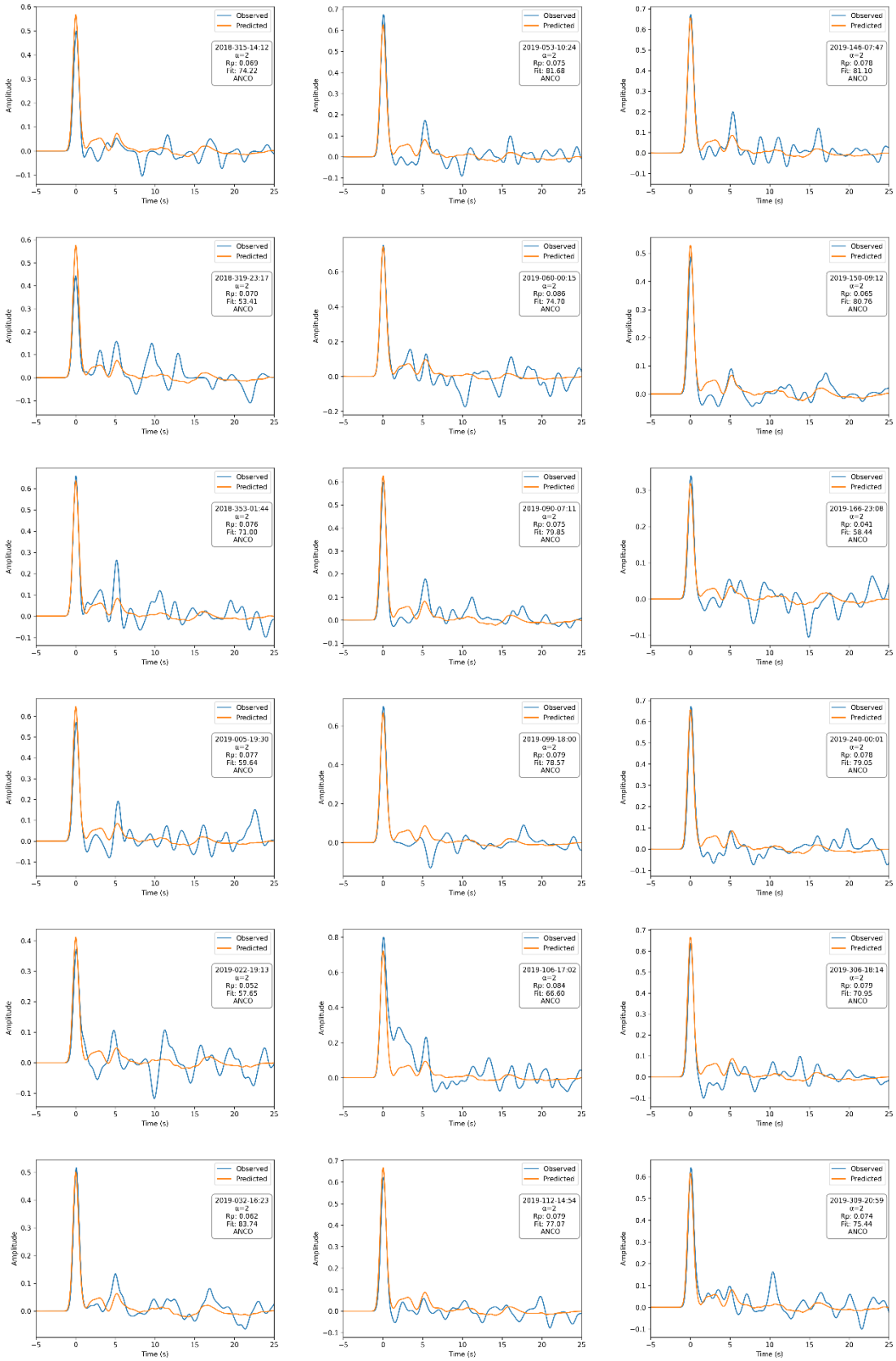

Figure S5: Observed (light blue line) and predicted (orange line) receiver functions fit of station ANCO.

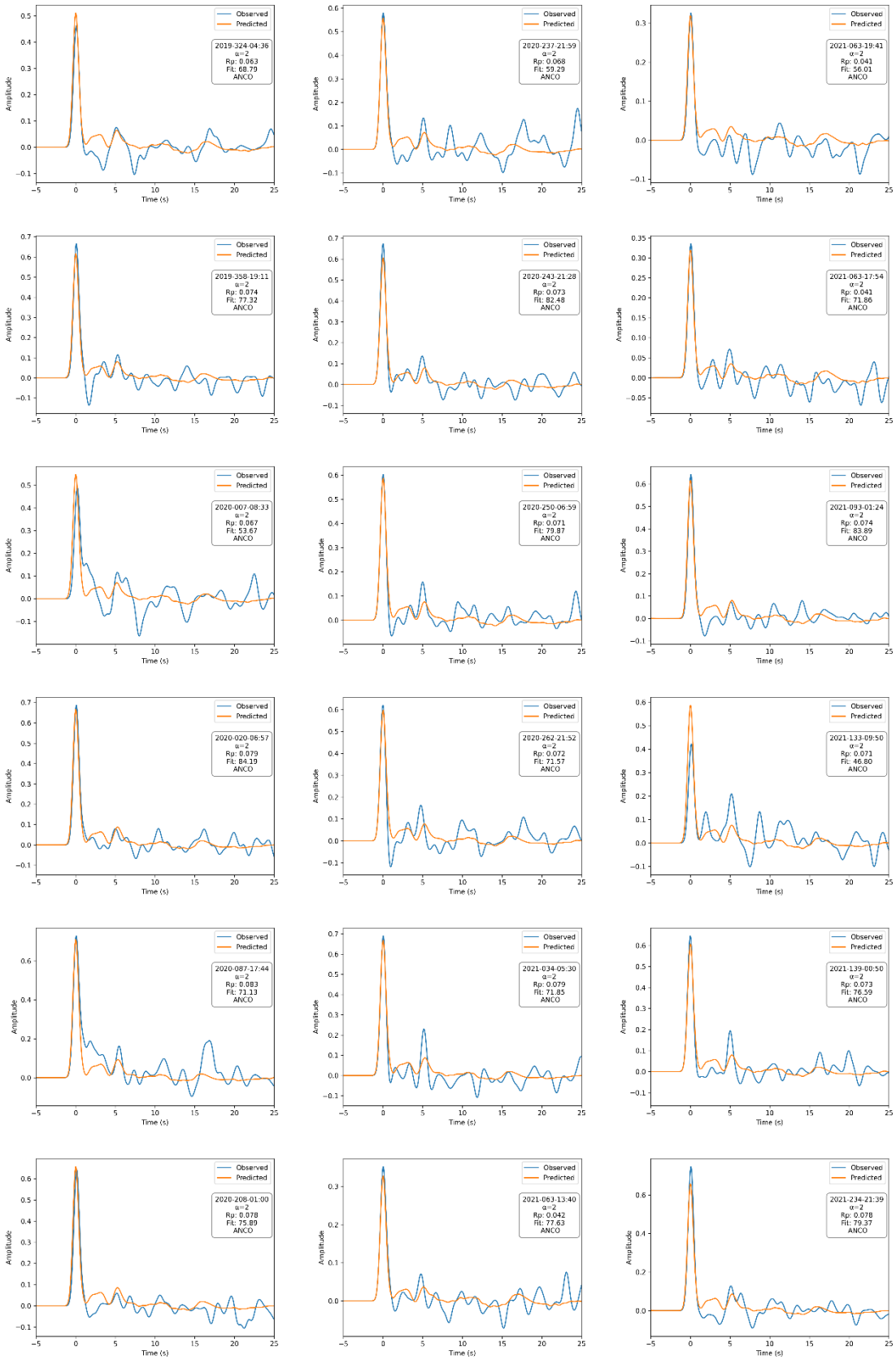

Figure S5 (continued)

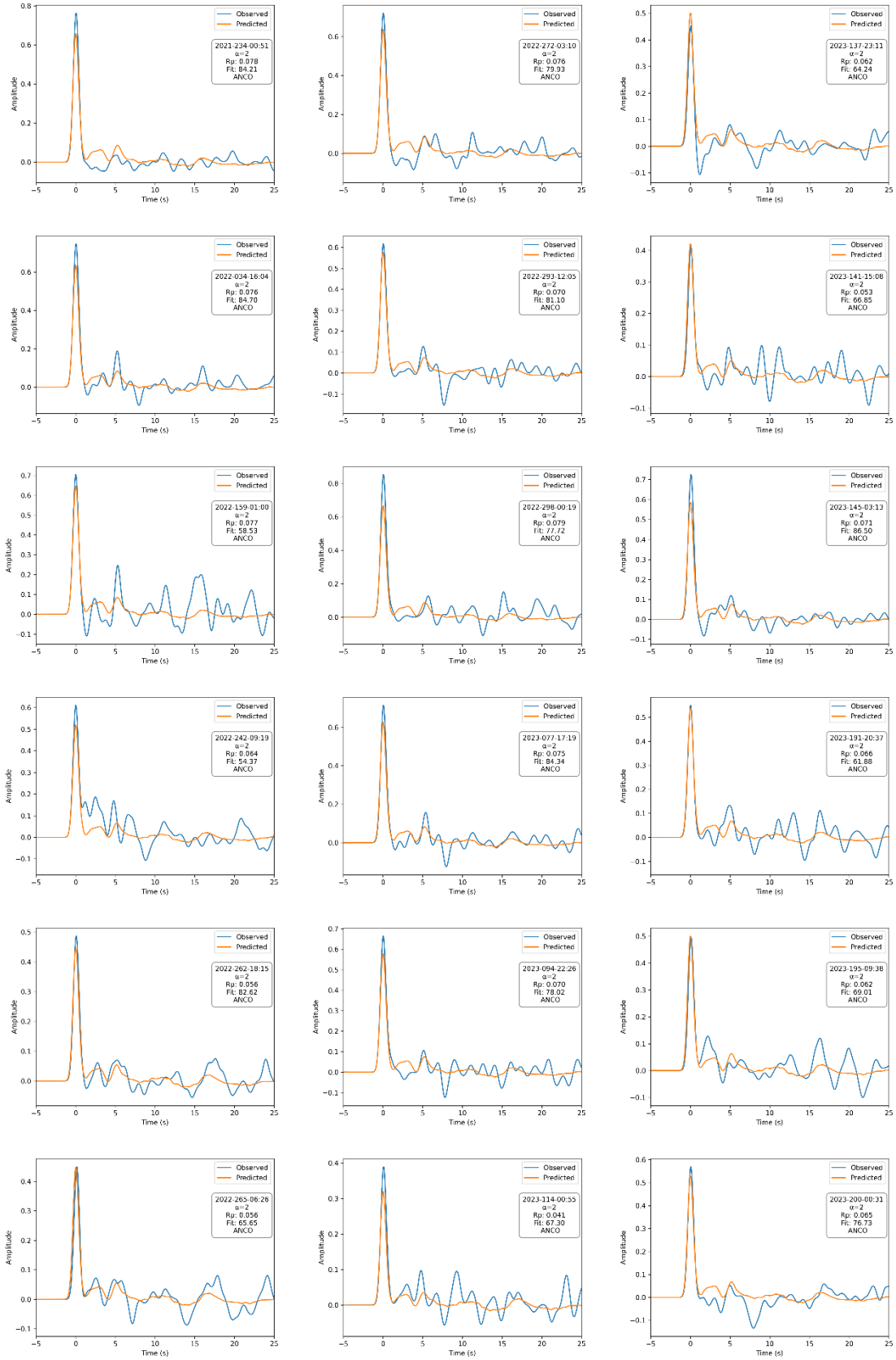

Figure S5 (continued)

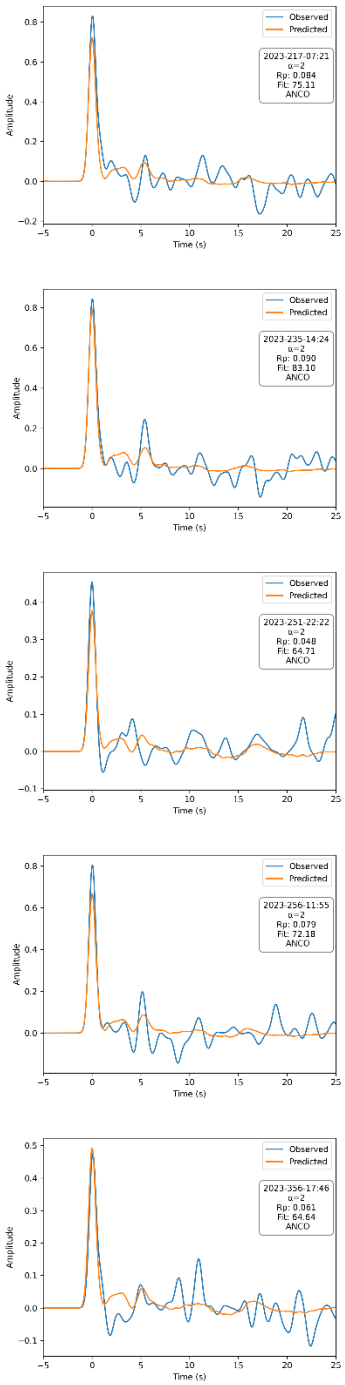

Figure S5 (continued)

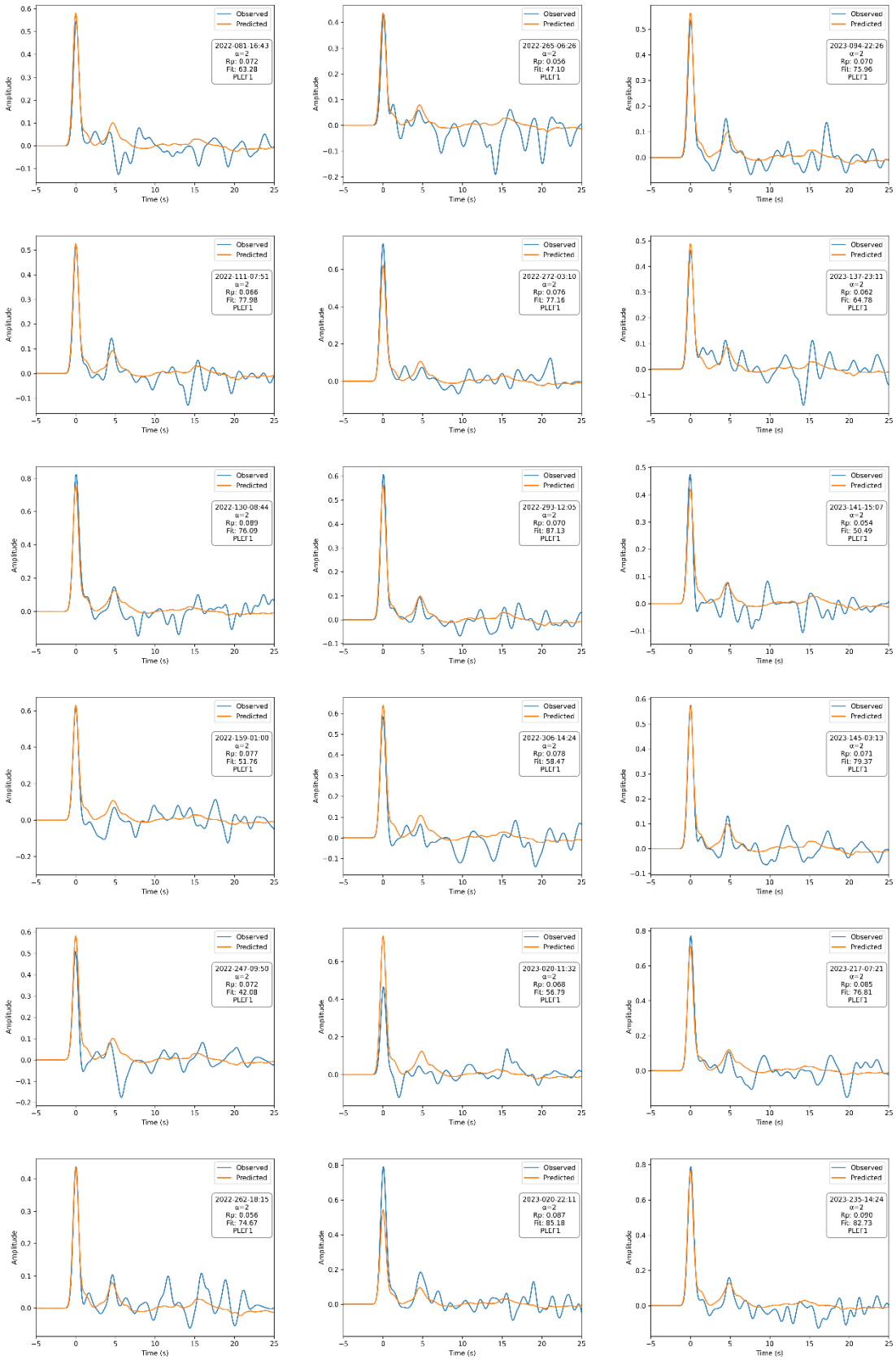

Figure S6: Observed (light blue line) and predicted (orange line) receiver functions fit of station PLEF1.

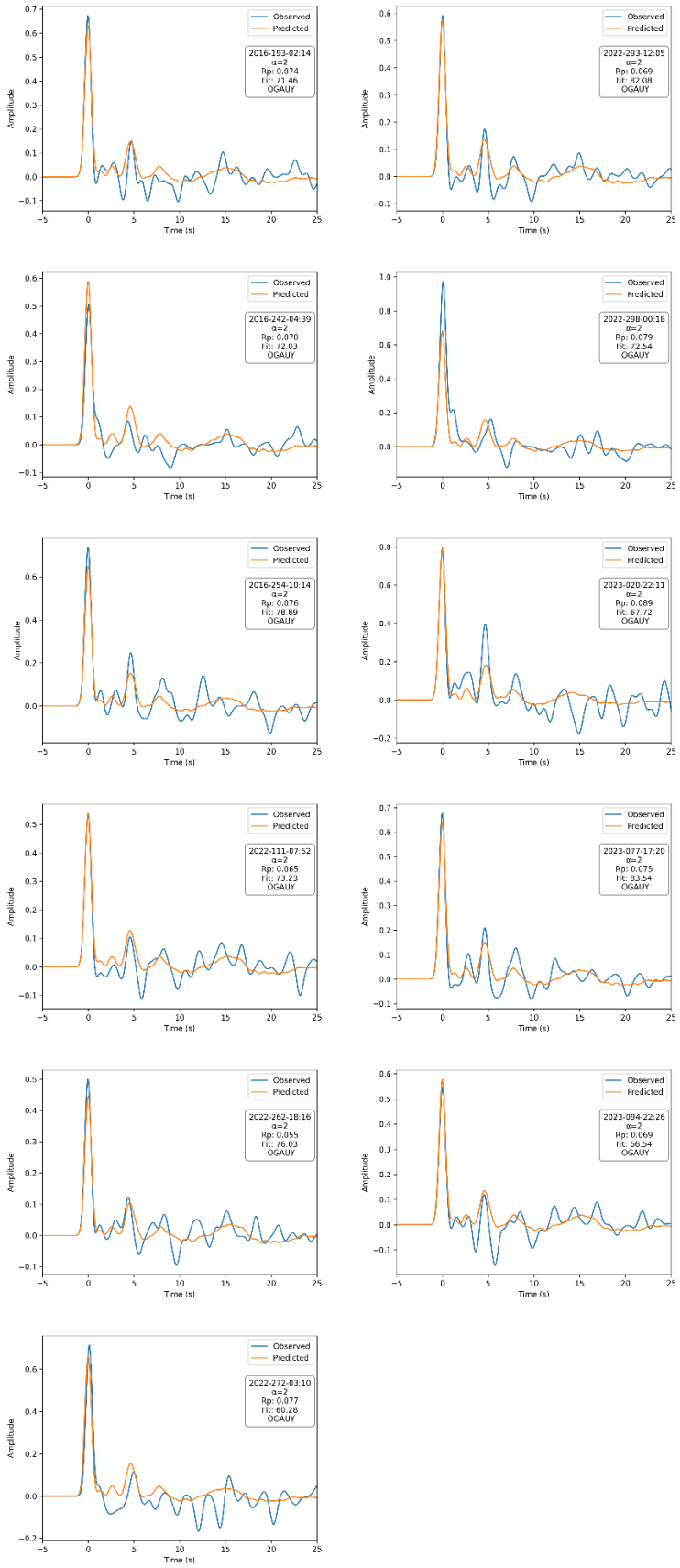

Figure S7: Observed (light blue line) and predicted (orange line) receiver functions fit of station OGAUY.

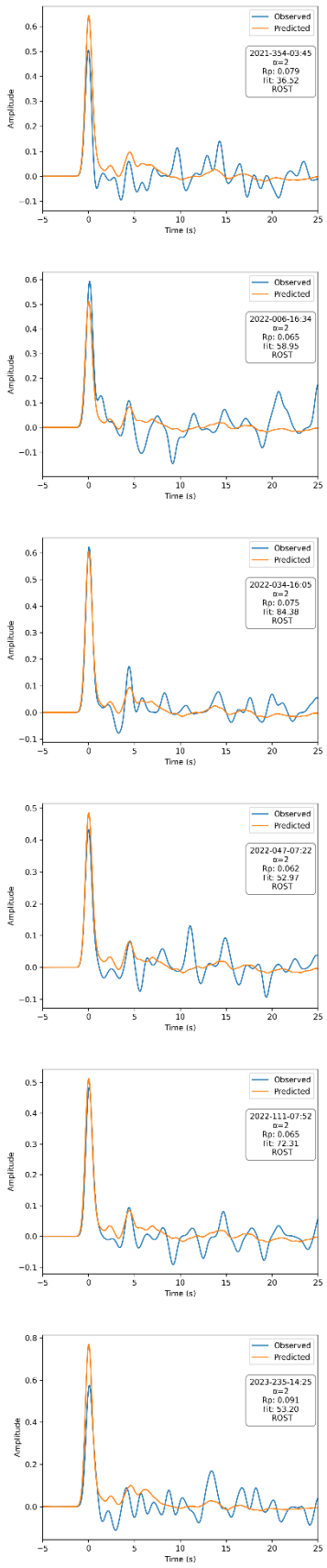

Figure S8: Observed (light blue line) and predicted (orange line) receiver functions fit of station ROST.

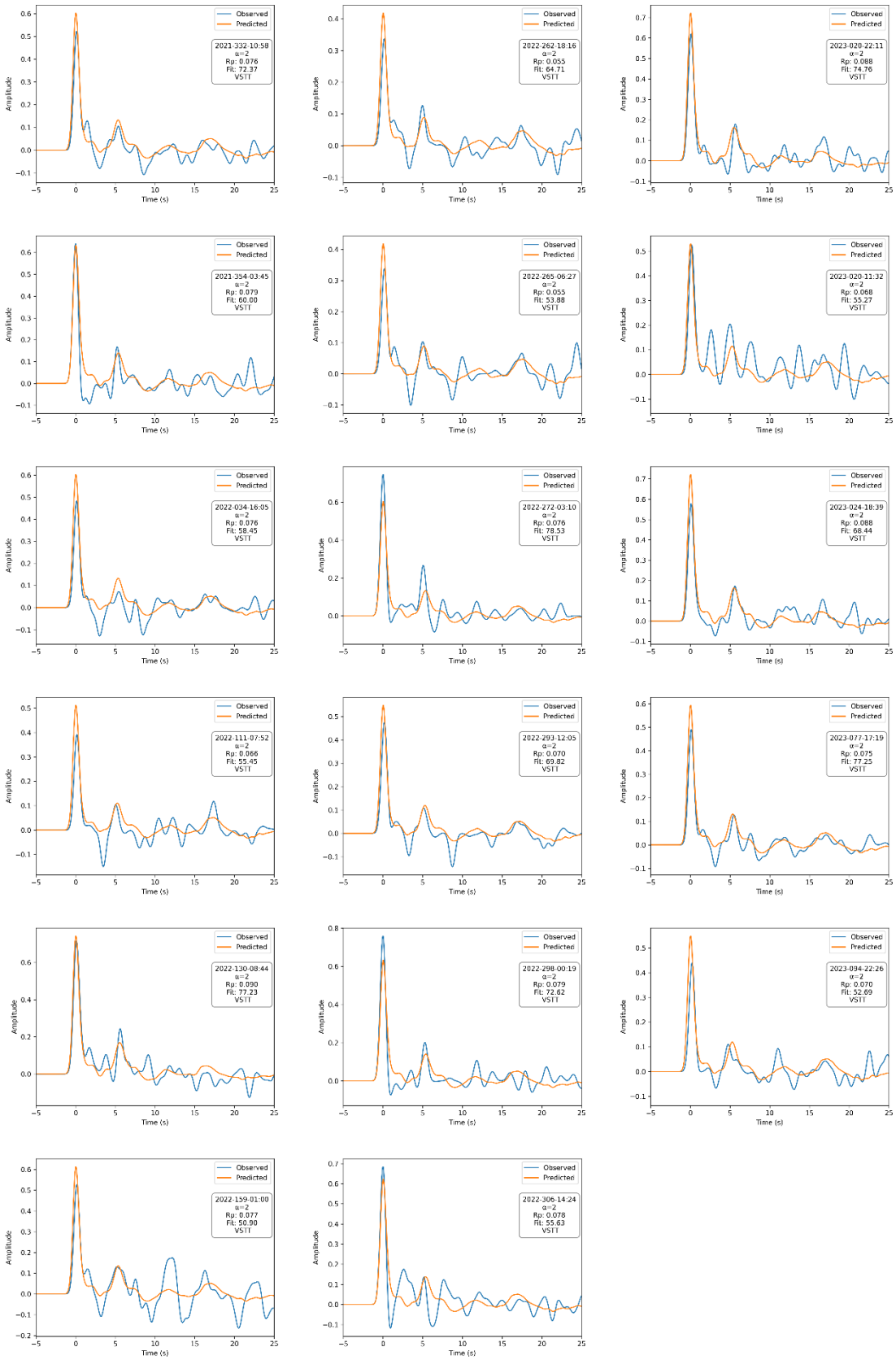

Figure S9: Observed (light blue line) and predicted (orange line) receiver functions fit of station VSTT.

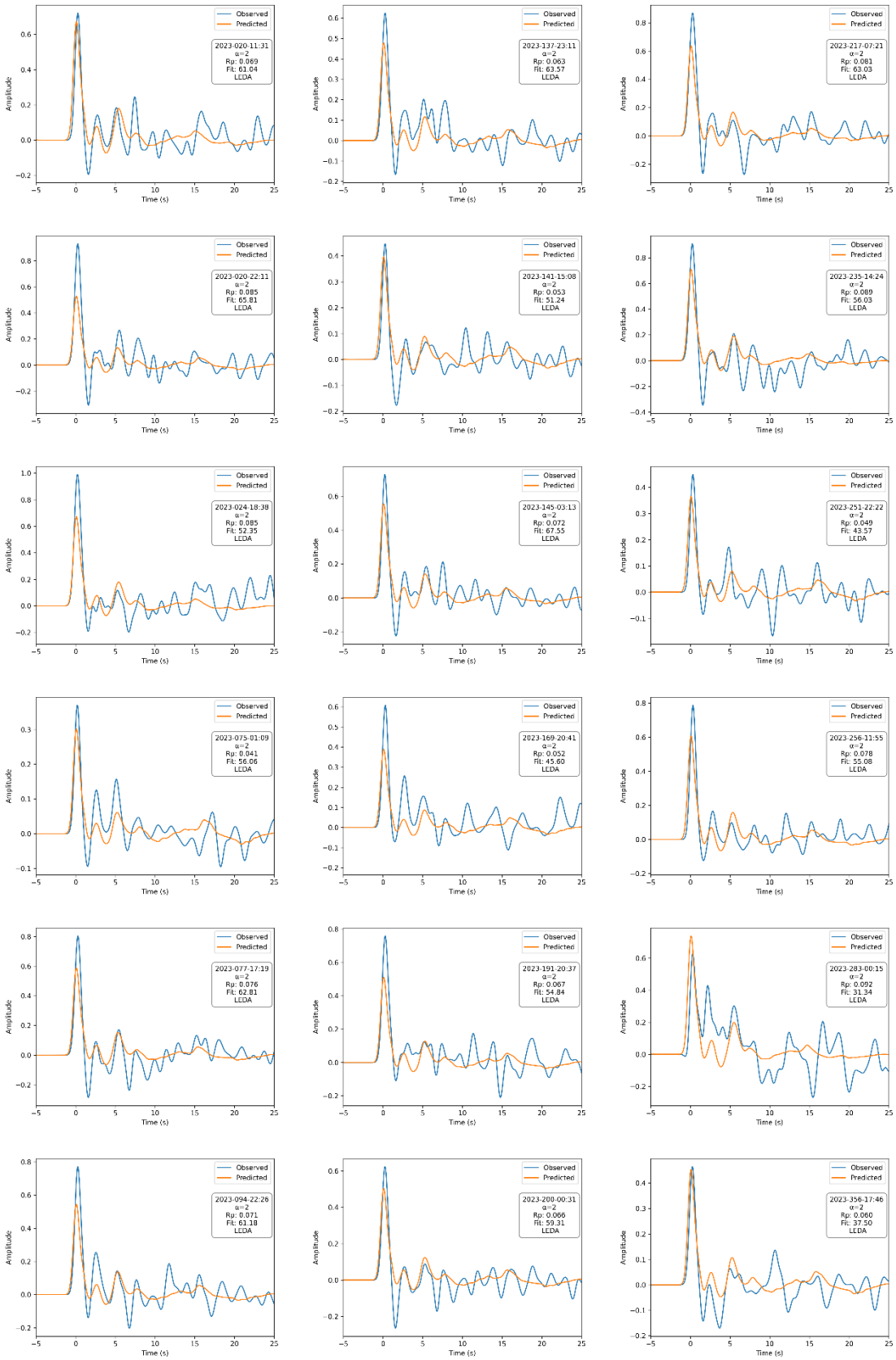

Figure S10: Observed (light blue line) and predicted (orange line) receiver functions fit of station LEDA.

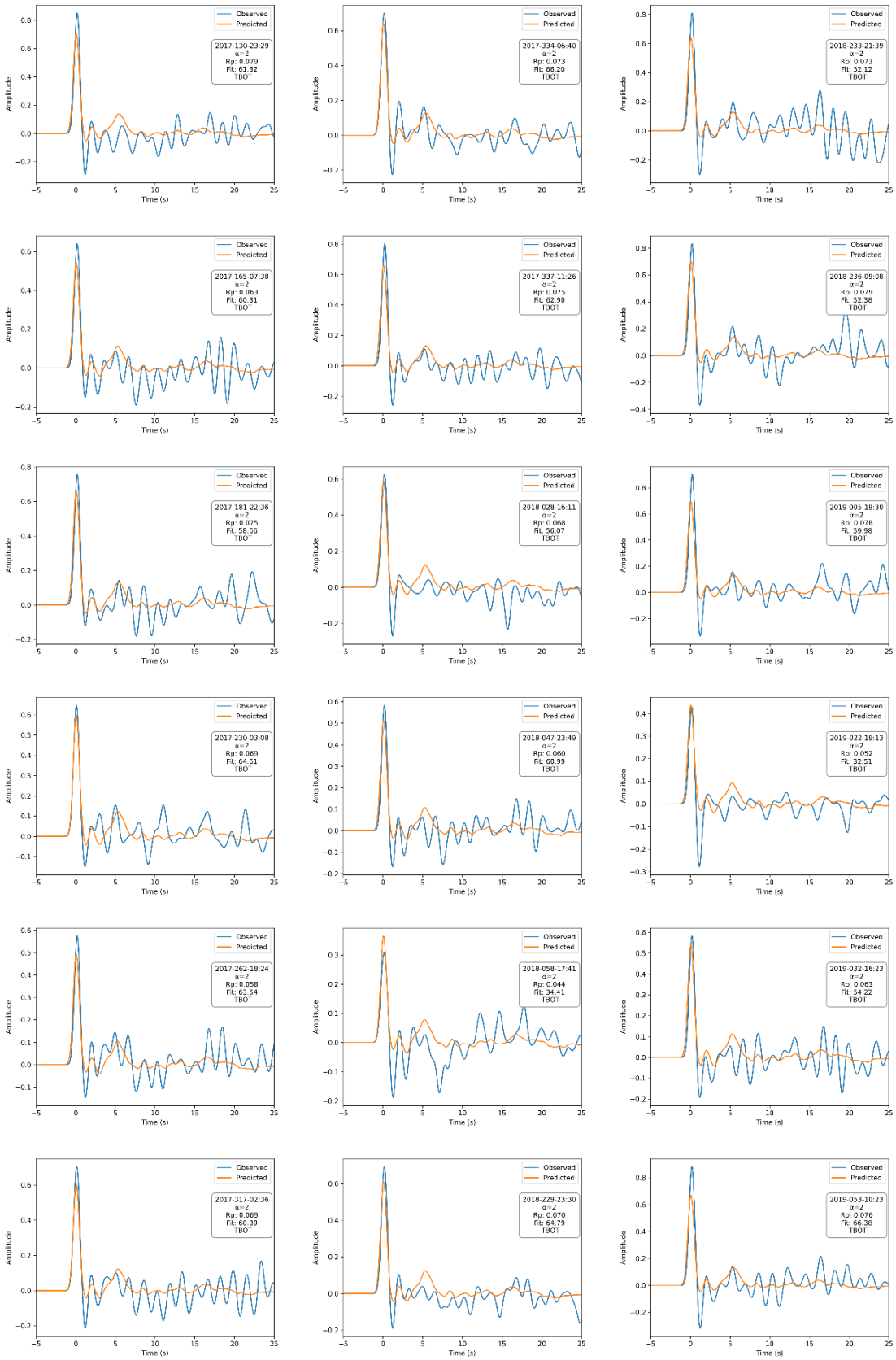

Figure S11: Observed (light blue line) and predicted (orange line) receiver functions fit of station TBOT.

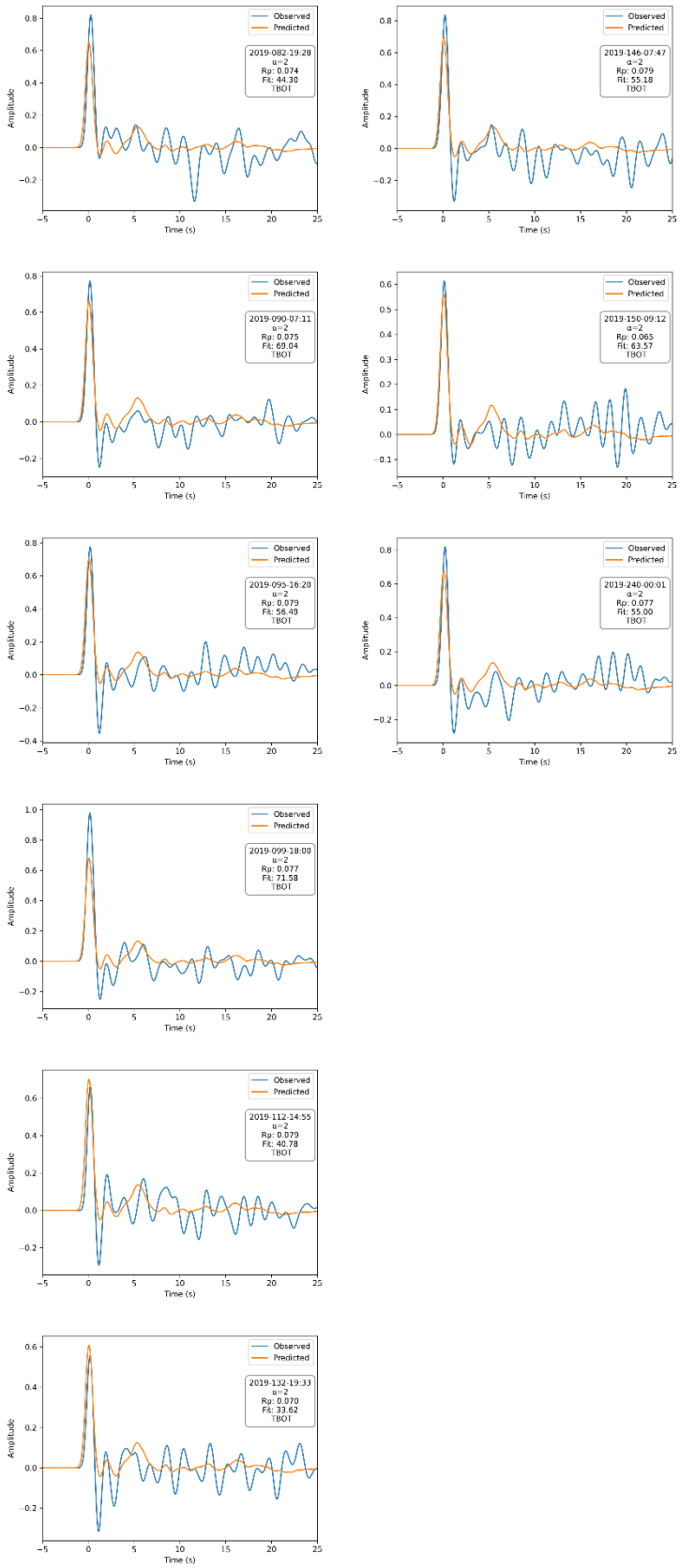

Figure S11: Observed (light blue line) and predicted (orange line) receiver functions fit of station TBOT.

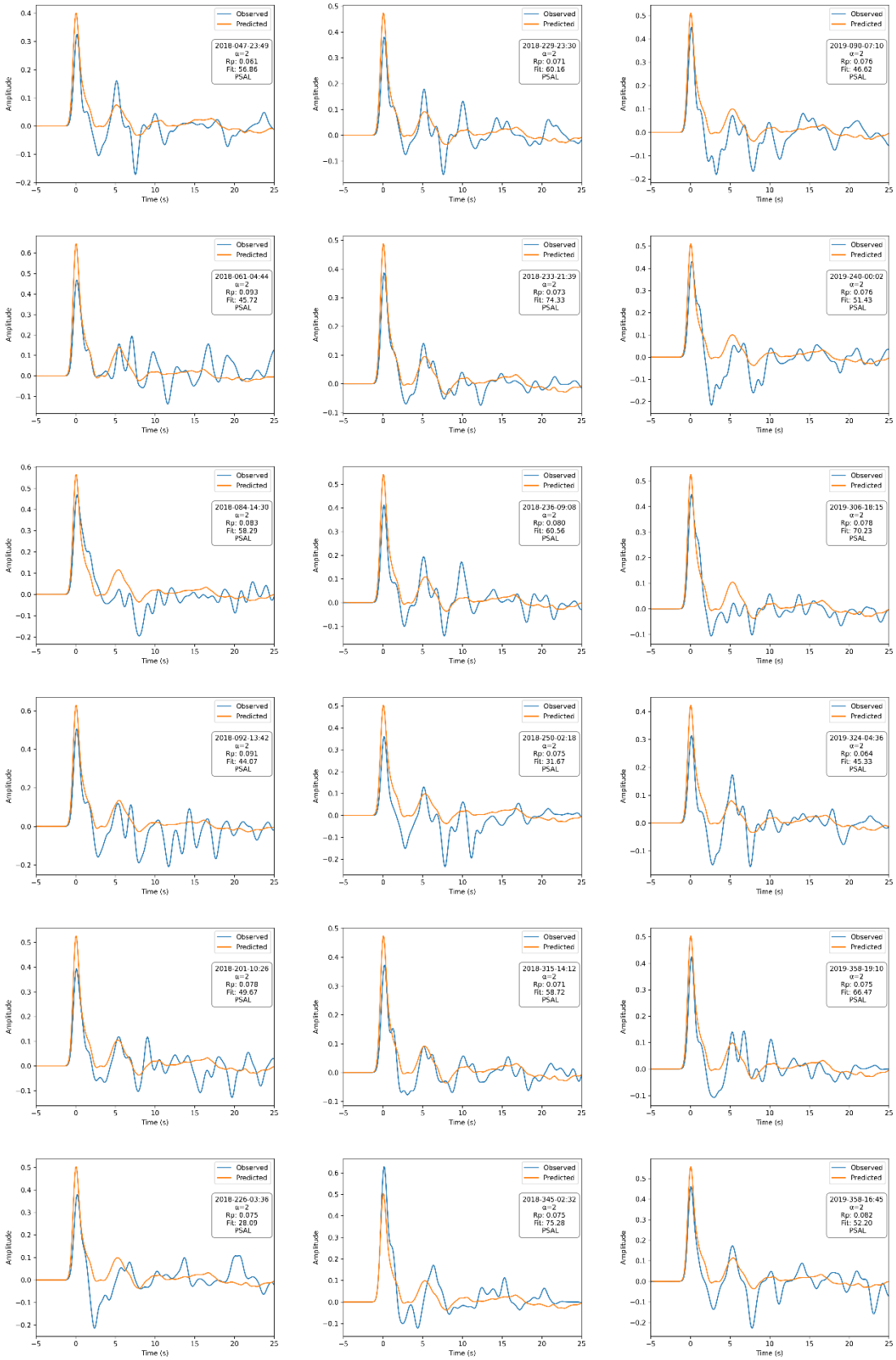

Figure S12: Observed (light blue line) and predicted (orange line) receiver functions fit of station PSAL.

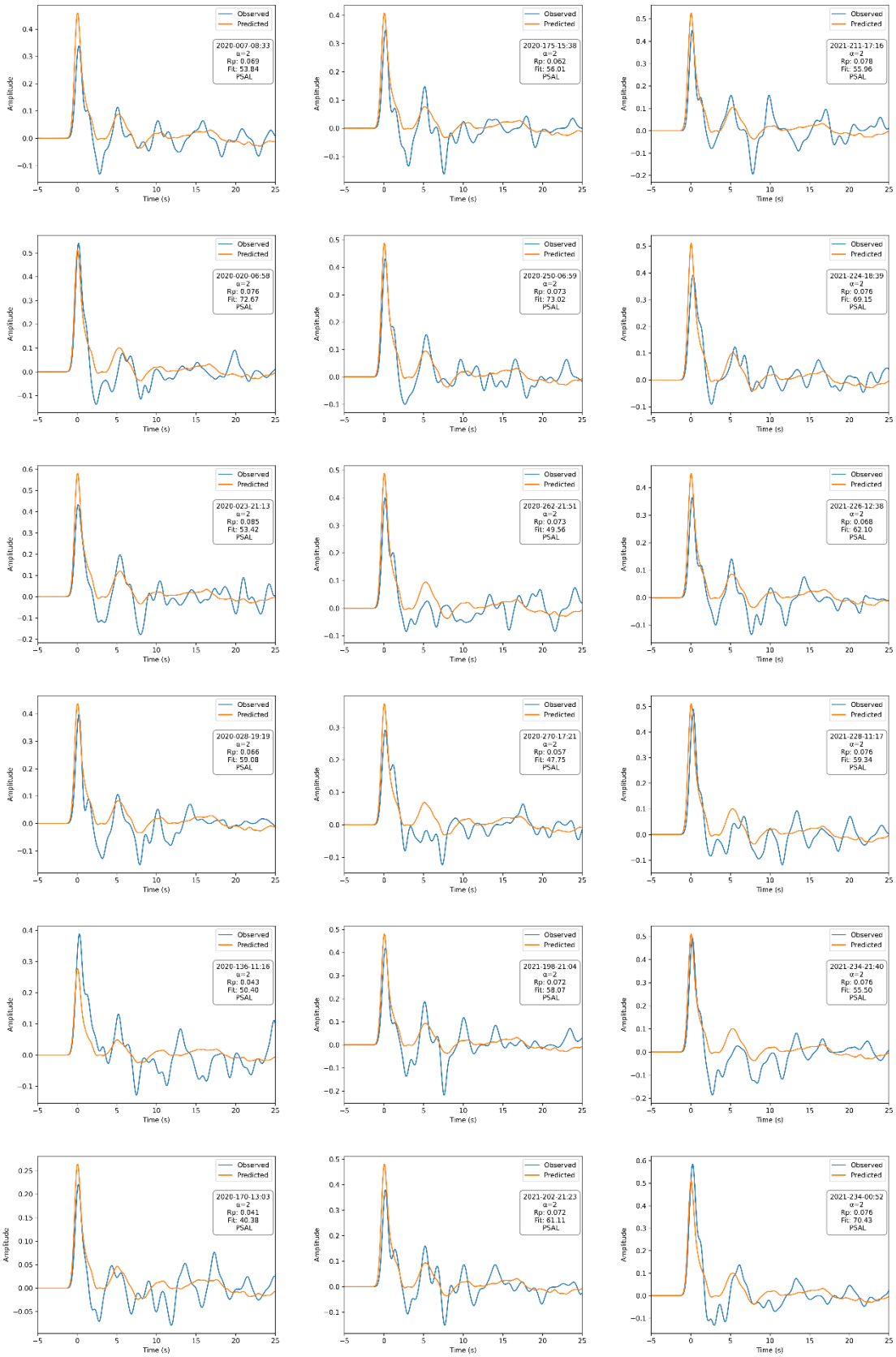

Figure S12 (continued)

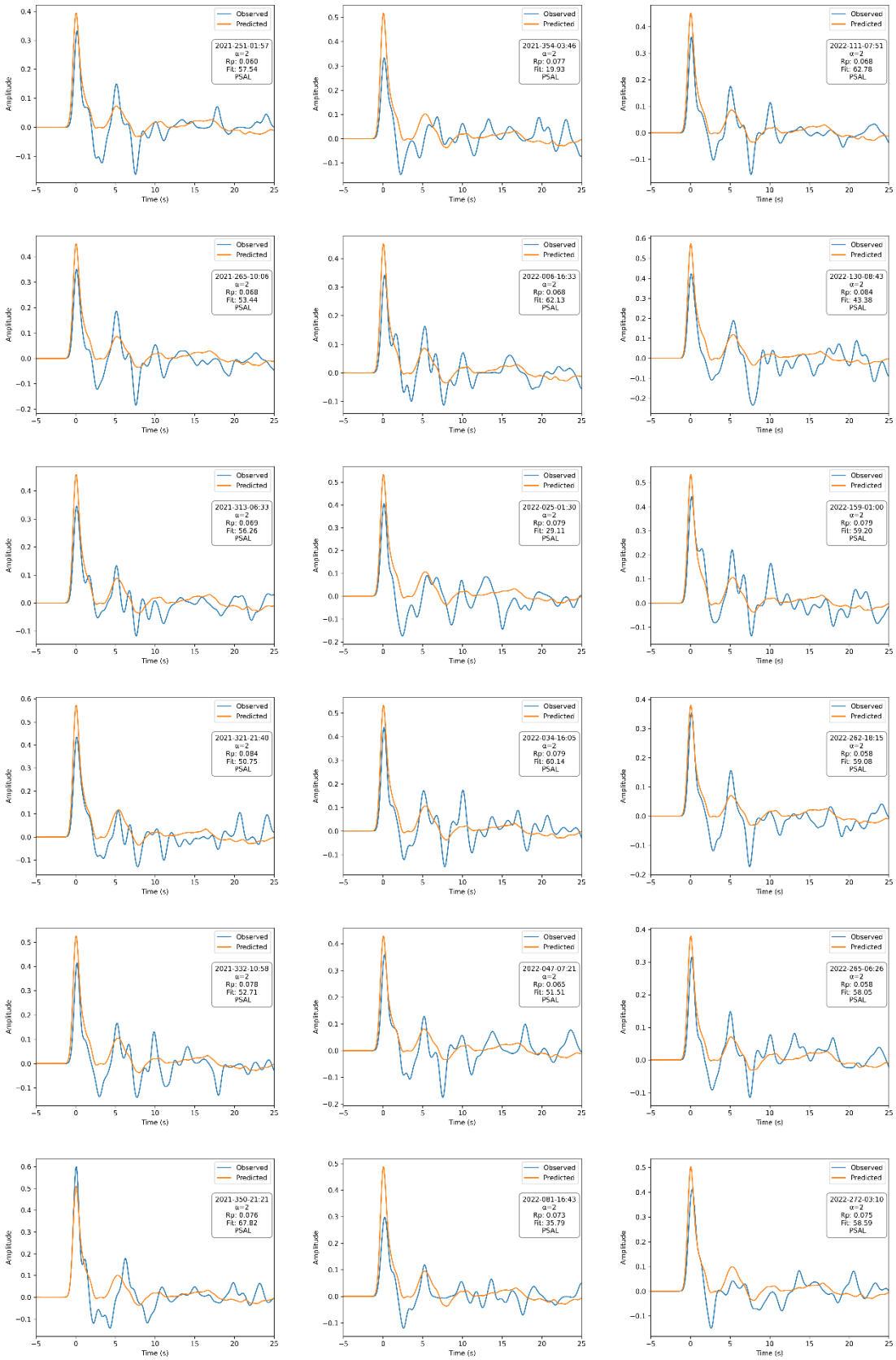

Figure S12 (continued)

Figure S12 (continued)